Articles

Site-Directed Mutants of Pseudoazurin: Explanation of Increased Redox Potentials from X-ray Structures and from Calculation of Redox Potential Differences[†,‡]

Clare Ann Peters Libeu,[§] Mutsuko Kukimoto,[||] Makoto Nishiyama,[||,⊥] Sueharu Horinouchi,[||] and Elinor T. Adman*[,§]

Department of Biological Structure, University of Washington, Box 357420, Seattle, Washington 98195-7420, and Department of Biotechnology, University of Tokyo, Yayoi 1-1-1, Bunkyo-ku, Tokyo 113, Japan

Received February 21, 1997; Revised Manuscript Received August 1, 1997[⊗]

ABSTRACT: In order to understand the origins of differences in redox potentials among cupredoxins (small blue type I copper-containing proteins that reversibly change oxidation state and interact with redox partners), we have determined the structures of the native and two mutants (P80A and P80I) of pseudoazurin from *Alcaligenes faecalis* S-6 in oxidized and reduced forms at resolutions of 2.2 Å in the worst case and 1.6 Å in the best case. The P80A mutation creates a surface pocket filled by a new water molecule, whereas the P80I mutant excludes this water. Distinct patterns of change occur in response to reduction for all three molecules: the copper position shifts, Met 7 and Pro 35 move, and the relative orientations of residues 81 to 16, 18 to the amide planes of 77 and 86, all change. Systematic changes in the weak electrostatic interactions seen in the structures of different oxidation states can explain the Met 7/Pro 35 structural differences as well as some fluctuating solvent positions. Overall displacement parameters increase reversibly upon reduction. The reduced forms are slightly expanded over the oxidized forms. The geometries of the mutants become more trigonal in their reduced forms, consistent with higher redox potentials (+409 mV for P80A and +450 mV for P80I). Calculations of the differences in redox potentials, using POLARIS, reveal that a water unique to the P80A mutant is required (with correctly oriented hydrogens) to approximate the observed difference in redox potential. The POLARIS calculations suggest that the reduced forms are additionally stabilized through changes in the solvation of the copper center, specifically via the amides of residues 16, 39, 41, 79, and 80 which interact with either Phe 18, Met 86, or Cys 78. The redox potential of P80A is increased largely due to solvation effects, whereas the redox potential of P80I is increased largely due to geometrical effects.

Pseudoazurin is a small electron transfer protein which is thought to participate in the denitrification pathway of the soil bacteria *Alcaligenes faecalis*. It was originally isolated as a factor which inactivates a copper-containing nitrite reductase from the same organism in the presence of reducing agents such as ascorbate under aerobic conditions (Kakutani et al., 1981). Similar pseudoazurin−nitrite reductase systems have also been reported from several other bacterial species including *Achromobacter cycloclastes* (Shapleigh & Payne, 1985). In a third species, *Thiosphaera pantotropha*, pseudoazurin has been implicated as an electron acceptor of hydroxylamine oxidase, which is a key enzyme in a nitrification pathway and may act to couple nitrification and denitrification pathways in this organism (Wehrfritz et al., 1993). Like plastocyanin in photosynthesis, pseudoazurin appears to function as a soluble electron shuttle between complex systems of electron transport chains.

Also like plastocyanin, pseudoazurin is a member of the cupredoxin family of electron transfer proteins. Cupredoxins are small type I copper-containing electron transfer proteins (10−14 kDa) whose active sites are characterized by an intense absorption near 600 nm and unusually small hyperfine coupling constants for the paramagnetic [oxidized, Cu(II)] forms of the proteins. The redox potentials of cupredoxins vary between 187 mV for stellacyanin and 670 mV for rusticyanin (Sykes, 1990). This large variation in redox potential is intriguing because the structure of the redox center in cupredoxins appears to be highly conserved. High-resolution X-ray structures (>2.0 Å) are known for seven cupredoxins: azurin, amicyanin, pseudoazurin, plastocyanin, cucumber basic blue protein, stellacyanin, and rusticyanin (Baker, 1988; Durley et al., 1993; Adman et al., 1989; Petratos et al., 1988; Inoue et al., 1994; Collyer et al., 1990; Guss et al., 1986; Hart et al., 1996; Walter et al., 1996). Although the sequence identity of the cupredoxins is very low (<20%) (Adman, 1991), all of these proteins fold into a characteristic β-barrel in which the copper ligands are positioned by a network of hydrogen bonds in analogous places. In each of these structures, the coordination of the copper is intermediate between tetrahedral and trigonal with an axial Met on the copper side of the plane formed by two

[†] Supported in part by NIH Grant GM31770 to E.T.A. and Training Grant in Molecular Biophysics GM0826 to C.A.P.L.

[‡] Coordinates for the structures reported herein have been deposited in the Brookhaven Protein Data Bank with PDB codes 3paz, 4paz, 5paz, 6paz, 7paz, and 8paz.

* Corresponding author. Tel: (206) 543-6589. FAX: (206) 543-1524. E-mail: adman@u.washington.edu.

[§] University of Washington.

[||] University of Tokyo.

[⊥] Present address: Biotechnology Research Center, University of Tokyo, Yayoi 1-1-1, Bunkyo-ku, Tokyo 113, Japan.

[⊗] Abstract published in *Advance ACS Abstracts,* October 1, 1997.

S0006-2960(97)00411-X CCC: $14.00

histidine nitrogens and a cysteine sulfur. Spectroscopic studies are consistent with the fact that the geometry of the copper−cysteine (bond length, 2.13 ± 0.06 Å; torsion angles, Cu−S^{γ}−C^{β}−C^{α} ∼−170° and S^{γ}−C^{β}−C^{α}−N ∼ 170°) is one of the most highly conserved features of the cupredoxins (Han et al., 1991). The ligand positions are virtually unaffected by removal (Garrett et al., 1984; Shepard et al., 1993; Petratos et al., 1995) or replacement of the copper with either mercury (Church et al., 1986) or cadmium (Blackwell et al., 1994), indicating that the protein architecture of cupredoxins is not dependent upon the copper ion but rather that the unique coordination of the copper is imposed by the protein architecture. Similarly, the coordination of the copper center is preserved upon reduction at physiological pH (Guss et al., 1986; Shepard et al., 1990; Vakoufari et al., 1994; Libeu & Adman, 1997). Fee and Malmström (1968) proposed that this restraint of the ligands into the distorted tetrahedral arrangement, which is unfavorable for Cu^{I}, accounts for the positive redox potentials of cupredoxins as well as their characteristic blue color and unusual hyperfine splitting. The high conservation of the copper center geometry and stability of the copper center upon reduction in cupredoxins make it likely that the variation in redox potentials among the cupredoxins is caused by differential solvation of the copper center by the nonligand protein atoms and solvent molecules (Sykes, 1990).

A network of hydrogen bonds from the rest of the protein residues is thought to restrain the copper ligands to their characteristic geometry. We have produced a series of single site mutants of pseudoazurin from *A. faecalis* in order to probe the effect of the hydrogen-bonding network on the geometry and redox potential of the copper center and have chosen two for structural and theoretical characterization. One consistent difference between the plastocyanin-like cupredoxins such as amicyanin and pseudoazurin and the azurins is that, in all plastocyanin-like cupredoxins, a proline immediately precedes the second histidine ligand. The presence of this proline precludes formation of a hydrogen bond found between the amide nitrogen of this residue and the cysteine sulfur in the azurins. The P80A[1] mutation was predicted to allow formation of this hydrogen bond; however, a new water molecule fills the hole left by the proline (Nishiyama et al., 1992), and the amide N−H is directed between the water oxygen and the cysteine sulfur. This small structural change is associated with a 139 mV increase in redox potential, one of the largest changes in redox potential observed for a single site cupredoxin mutant. A second mutation, P80I, was engineered in order to displace the new water molecule and allow the hydrogen bond to form. The redox potential of this mutant is even higher, with an increase in redox potential of 180 mV, indicating that the type of residue found at this position heavily influences the redox potential of pseudoazurin.

It has been shown previously (Langen et al., 1992) that the energy of oxidation of a redox protein can be treated as the sum of the energy of oxidation of the redox center in the gas phase and the differences in the energy of interaction in two oxidation states of that redox center with its protein plus solvent surroundings, or "solvation energy". Differences in redox potentials can then be approximated by differences in these solvation energies. In order to interpret the effects of the two mutations of Pro 80 on the redox potential, we have determined the structure of both oxidation states for native, P80A, and P80I pseudoazurin and also calculated the solvation energy for all six forms.

EXPERIMENTAL PROCEDURES

(A) Preparation of Native and Mutant Pseudoazurin. The methods used to engineer and purify pseudoazurin and ten mutants are described in Kukimoto et al. (1995) and Nishiyama et al. (1992).

(B) Measurement of Redox Potentials. Measurement of redox potentials was carried out as in Nishiyama et al. (1992) by redox titration with ascorbate or ferricyanide, measuring absorbance at 593 nm.

(C) Crystallization. Brilliant blue hexagonal bipyramidal crystals of the oxidized forms of all three pseudoazurins were obtained from 50 mM Na_2HPO_4 buffer with 75% saturated ammonium sulfate (Kakutani et al., 1981). All three pseudoazurins crystallize in space group $P6_5$. The P80A and native pseudoazurin crystals have the same cell dimensions as reported earlier for native pseudoazurin (Adman et al., 1989) (Table 1); however, the cell dimensions of P80I pseudoazurin differ slightly due to rotation of the molecule in the unit cell.

(D) Reduction and Reoxidation of Crystals. The native reduced crystals were generated by transferring crystals into 10 mM sodium ascorbate, 50 mM Na_2HPO_4 buffer, and 75% saturated ammonium sulfate at either pH 7.0 or pH 5.5.[2] Complete reduction of a 1.5 mm thick pyramidal crystal takes about 45 min. Crystals treated with 10 mM ascorbate generally cracked and split into two pieces, so that the larger of the pieces was selected for mounting. Reduced native crystals mounted in capillaries sealed with silicone oil turned a faint blue within 48 h, indicating that a small amount of the protein reoxidizes during data collection. However, a complete data set could be collected in just over 24 h at which point the crystals were still colorless.

P80A pseudoazurin crystals were reduced with 3 mM ascorbate, 50 mM Na_2HPO_4 buffer, and 75% ammonium sulfate (pH 7.0) and mounted in an anaerobic environment using degassed solutions, and the capillaries were sealed with wax. Reduced P80A crystals in sealed capillaries remained colorless for 2 weeks of storage at 4 °C, followed by more than 1 week at room temperature. After data collection, the reduced P80A crystals were removed from the capillaries and reoxidized with 10 mM $Fe(CN)_6$, 50 mM Na_2HPO_4 buffer, and 75% ammonium sulfate (pH 7.0). After 45 min in $Fe(CN)_6$ solution, the reoxidized crystals were rinsed with 50 mM Na_2HPO_4 buffer and 75% ammonium sulfate (pH 7.0) and then left to soak for 3 h in fresh buffer before being remounted. At the end of the soaking period, the brillant blue color typical of the oxidized crystals was restored.

P80I crystals were reduced with 3 mM ascorbate, 50 mM Na_2HPO_4 buffer, and 75% saturated ammonium sulfate. Reoxidation of the reduced P80I crystals is extremely slow. These crystals remain colorless up to 3 months when stored at 4 °C and for 3−4 weeks at room temperature. No detectable color changes were observed during data collection on the reduced crystals.

[1] Mutants are designated by a one-letter code of the wild-type residue type, residue position, and a one-letter code of the new residue type; e.g., Pro 80 Ala is P80A. esd is the estimated standard deviation.

[2] All pH's cited are the pH of the combined solution measured against a KCl electrode.

Table 1: Data Collection Statistics

single crystals	detector[a]	cell dimensions[b] *a* (Å)	cell dimensions[b] *c* (Å)	⟨*I*/σ(*I*)⟩ mean	⟨*I*/σ(*I*)⟩ limit	R_{merge} mean	R_{merge} limit	refl
oxidized native								
A[c]	Siemens	49.87	98.86	17.9	5.8	0.053	0.15	39 144
B	Siemens	50.38	98.98	17.9	3.6	0.062	0.14	23 642
C	Siemens	50.17	98.32	24.1	2.6	0.042	0.20	48 276
reduced native, pH 7.0								
A[c]	Siemens	49.92	98.84	50.2	10.6	0.032	0.10	30 604
B	Siemens	50.29	99.03	17.3	2.0	0.030	0.19	37 580
reoxidized native								
A	Siemens	50.15	98.78	15.2	3.58	0.033	0.07	10 928[d]
oxidized P80A								
A[c]	Siemens	50.0	98.36	23.8	8.4	0.040	0.12	28 427
B	Siemens	50.36	98.66	24.1	6.9	0.024	0.10	26 591
reduced P80A								
A	Siemens	50.02	98.42	27.0	10.7	0.06	0.11	13 743
B	Siemens	49.97	98.48	18.7	3.0	0.05	0.10	26 684
reoxidized P80A								
A	Siemens	50.05	98.54	23.7	3.9	0.038	0.08	25 025
B	Siemens	49.98	98.43	21.8	7.0	0.028	0.06	14 381
oxidized P80I								
A	Siemens	50.79	98.24	20.7	3.4	0.033	0.11	58 828
reduced P80I								
A	RAXIS	50.79	98.25	-na-	>3.0	>0.05	>0.15	27 000

[a] Each detector was used with a Rigaku RU200 rotating anode. For the Siemens data sets, individual reflections were integrated using XENGEN (Howard et al., 1987). RAXIS software (Higashi, 1990) was used for RAXIS-II image plate data. [b] $a = b$, α, $\beta = 90.0°$, and $\gamma = 120.0°$. [c] Data sets collected and processed by Stewart Turley. [d] There are 6378 unique reflections. The data are approximately 60% complete in the range 40−2.0 Å with the missing reflections distributed throughout the resolution range.

Table 2: Merged Data Sets Used for Refinement[a]

	crystals	d_{min}[b]	d_{max}[b]	%[c]	$I/\sigma(I)$	R_{merge}[d]	unique refl
oxidized native	3	26.20	1.6	88/65	8.7	0.044	18 528
reduced native	2	22.30	1.73	87/54	7.0	0.040	12 220
oxidized P80A	4	26.17	1.76	86/55	8.3	0.034	12 172
reduced P80A	2	10.29	1.76	84/48	10.0	0.046	10 723
reoxidized P80A	2	10.09	1.75		23.6	0.027	9 669
oxidized P80I	1	18.26	1.91	97/80	20.4	0.038	10 151
reduced P80I	1	26.00	2.00	96/90	(∼10)	(∼0.06)	9 327

[a] The pH of all crystals was 7.0 except for oxidized native which was 6.5. [b] d_{min} and d_{max}, lowest resolution and maximum resolution (Å). [c] Percent completeness, overall/highest resolution shell. [d] $R_{merge} = \sum_{hkl}\sum_{i=1}^{n}|I_i(hkl) - \langle I(hkl)\rangle|/\sum_{hkl}\sum_{i=1}^{n}I_i(hkl)$.

(E) Data Collection and Processing. Table 1 summarizes cell dimensions and data collection statistics. For all data sets collected on the Siemens/Xentronix X-1000 area detector, interframe scaling and averaging of replicate reflections were accomplished with the bin-scaling program MACRO (Ethan Merritt, personal communication); for each data set, data from all settings from each crystal were scaled together. All data sets for a particular protein were then scaled together in order to minimize differences in the data due to small systematic errors such as absorption. Table 2 summarizes the final statistics for each of the data sets.

(F) Reversibility of Reduction in the Crystals. In order to determine whether reduction of the crystals was reversible, reduced P80A crystals were reoxidized with ferricyanide after data collection. As shown in Figure 1, the difference between data collected on the reoxidized P80A and oxidized P80A crystals is much smaller than the difference between data sets collected on oxidized and reduced P80A or P80I crystals. Although data are shown for only one experiment, the reoxidation experiment was repeated for P80A, and identical results were obtained. The experiment was not tried with P80I crystals due to limited material. The values of R_{merge} between the reoxidized and oxidized P80A data for each experiment are within the magnitudes of R_{merge} observed for replicates within each data set. The reversibility of the reduction of the pseudoazurin crystals indicates that the observed differences are due to oxidation state change and not crystal manipulation.

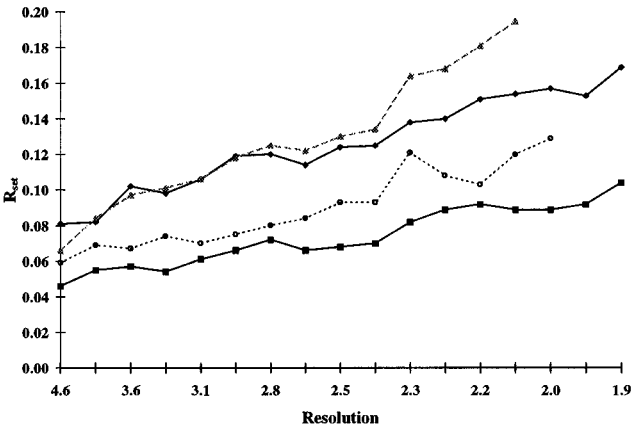

FIGURE 1: Agreement between the structure factors of oxidized P80A pseudoazurin and reoxidized P80A (■), oxidized native pseudoazurin and oxidized native pseudoazurin with a half-occupied copper (○), oxidized and reduced P80I pseudoazurin (▲), and oxidized and reduced P80A pseudoazurin (◆).

(G) Refinement. The published 2.0 Å oxidized native pseudoazurin model (PDB code 2paz) (Bernstein et al., 1977; Adman et al., 1989) without solvent molecules was used as the starting model for all structures. Rigid body refinement (X-PLOR; Brünger, 1990) was necessary to place the P80I

Table 3: Progress of Refinement

	oxidized native	reduced native	oxidized P80A	reduced P80A	oxidized P80I	reduced P80I
PROLSQ						
cycles	9	4	5	8	5	
R^a (<10 Å)	0.169	0.176	0.166	0.176	0.175	
σ (bonds)	0.028	0.021	0.024	0.022	0.019	
water molecules	73	71	85	87	47	
X-PLOR						
cycles	3	3				8
R (<10 Å)	0.166	0.164				0.186
σ (bonds)	0.025	0.023				0.010
water molecules	83	98				46
alternate side chains	9	9				
SHELXL-95						
cycles	7	5	5	5	4	4
starting parameters	4215	4285	4065	4073	3917	3913
finish parameters	4205	4279	4045	4077	3994	3882
bulk solvent[b]	4.59	4.90	4.45	4.24	4.03	4.48
water molecules	58	89[c]	71	79	53	38
alternate side chains	10	6				
av dev bond (Å)	0.007	0.006	0.006	0.006	0.005	0.004
av dev angle (deg)	0.019	0.019	0.019	0.019	0.016	0.018
R (all data)	0.178	0.165	0.167	0.170	0.192	0.210
R ($I/\sigma(I) > 4$)	0.167	0.158	0.157	0.163	0.175	0.200
GOOF[d]	3.10	4.19	4.52	4.69	5.12	5.24
highest peak (e/Å^3)	0.33	0.18	0.68	0.34	0.22	0.34
av esd[e] (Å)	0.08	0.10	0.11	0.11	0.12	0.17
PDB code	8paz	3paz	4paz	5paz	6paz	7paz

[a] The R value is defined as $R = \sum_{hkl}||F_{o,hkl}| - |F_{c,hkl}||/\sum_{hkl}|F_{o,hkl}|$, where F_o is the observed structure factor and F_c is the calculated structure factor. The free R value is not reported in this paper because in the initial (PROLSQ and XPLOR) refinements every observed reflection had been used in the refinement and it was no longer possible to set aside an unused set of data. [b] In SHELXL, the bulk solvent is modeled using Babinet's principle by adding a correction to the real part of the scattering factor (f) of each non-hydrogen atom: $f(\text{new}) = f(\text{old}) - g\exp(-8\pi U(\sin\theta/\lambda)^2)$. g is the parameter given in the table; U is fixed at 2.0. [c] When the coordinates were deposited, we found that this solvent set still contains several effectively duplicate molecules related by symmetry operations and are noted as such in the coordinate entry. [d] The goodness of fit (GOOF) is defined as $\text{GOOF} = \text{SQRT}(\sum w_i(F_{oi}^2 - F_{ci}^2)^2/(N - p))$, where N is the number of reflections, p is the number of parameters, F_{oi}^2 is the observed intensity, and F_{ci}^2 is the calculated intensity of the ith reflection. w_i is the weight of the ith reflection and is defined as $w_i = 1.0/(\sigma_i^2(F_{oi}^2) + 0.1(2F_{ci}^2 + \max(F_{oi}^2,0))/3)$. w_i is the weight used for each reflection in the SHELXL refinement. All other refinements were done using unit weights. These particular weights are thought to reduce statistical bias (Wilson, 1976). [e] The average esd was calculated using the esd's from restrained full-matrix least squares refinement, for all atoms whose displacement parameters are less than 60 Å^2. Average esd $= (\epsilon_x^2 + \epsilon_y^2 + \epsilon_z^2)^{1/2}$, where ϵ_x, ϵ_y, ϵ_z are the mean esd's for their respective coordinate.

starting model in the unit cell before refinement was begun. The P80I molecule rotated about 1.2° relative to the native molecule.

The models were first refined by alternating cycles of restrained least squares conjugate gradient minimization implemented in PROLSQ (Hendrickson, 1985) or X-PLOR with model building on a IRIS workstation using the graphics program O (Jones et al., 1991). All $F_o - F_c$ and $2F_o - F_c$ difference electron density maps were calculated using the CCP4 suite of programs (CCP4, 1994). Although normal restraints were used on bond lengths and angles for the protein atoms in the PROLSQ refinement, neither the copper ligand bond distances nor angles were restrained. In X-PLOR, protein atoms were restrained using the Engh and Huber set of parameters (Engh & Huber, 1991), and copper−ligand distances and angles were not restrained. After a complete model of the fully occupied solvent was constructed for each structure, the models were transferred into SHELXL (Sheldrick, 1993), so that the copper and sulfur atoms could be refined anisotropically. SHELXL also uses the Engh and Huber parameters to generate restraints for the protein atoms. In the final cycles of refinement, a bulk solvent correction was applied.

In each refinement, a special effort was made to determine the positions of the water molecules independently. Candidate water molecules were identified by screening the 100 highest peaks in the $F_o - F_c$ map from each cycle of conjugate gradient minimization for appropriate distance (2.6−3.1 Å) and geometry (angles of 104−115°) for water molecules with multiple hydrogen bonds. Until the final stages of the refinement a water molecule was not accepted unless two potential hydrogen-bonding partners were available, its peak height in the $F_o - F_c$ difference map was above 4σ, and its displacement parameter value remained below 50 Å^2 in subsequent cycles of refinement. Before the last cycle of refinement, candidate water molecules from all structures were correlated and given consistent names. Relevant difference maps from each structure were then checked at sites of unique water molecules in the other three structures in order to determine whether the site was truly unoccupied or if the position was occupied by less well ordered water molecules. Peaks in the $F_o - F_c$ map above 2σ were interpreted as partially occupied water molecules but not included in the final models. Models of side chains with alternate conformations were refined with X-PLOR and then with SHELXL for both oxidized and reduced native pseudoazurin. Disordered side chains were treated in two ways. Large side chains, such as glutamates and lysines, were modeled as distinct conformations. However, extra electron density associated with some of the isoleucines, valines, and aspartates was better modeled by refining those side chains anisotropically. Although modeling the side chains using anisotropic displacement parameters adds additional parameters to the refinement, in fact the total number

of parameters used in the SHELXL refinement was less than the X-PLOR/PROLSQ refinements because fewer discrete water molecules were included. Because of the relatively poor resolution of the P80I models, no attempt was made to model alternate conformations or to refine atoms other than the copper and the sulfur atoms anisotropically. In all six models the copper and the sulfur atoms were refined anisotropically so that the orientation of the resulting thermal ellipsoids could be compared. Introduction of these parameters did not significantly improve the agreement between the calculated and observed reflections. Table 3 summarizes the path of refinement for each model as well as the final statistics.

The decrease in the number of discrete water molecules in the models after SHELXL refinement was not unexpected. Most of the water molecules omitted were either modeled as partially occupied or had relatively high displacement parameters. The application of the bulk solvent model effectively decreases the contrast at the solvent positions, so that only the best defined waters are apparent. This process does not result in any significant decrease in the overall agreement between calculated and observed reflections but seems to improve agreement for higher resolution shells. In all refinements, there are still peaks in the last ($F_o - F_c$) maps that may be partially occupied water molecules.

All final models were checked with the program PROCHECK (Laskowski et al., 1993) and had acceptable stereochemistry. Some surface side chains (K10, K24, E51, K54, E62, N63) associated with high displacement parameters had deviations in χ_1 of 20−40°. K46 was modeled as A46 throughout. A notable deviation of 12−14° in ϖ for peptide 77−78 persists in all six structures and is also seen in the native oxidized structure determined in another laboratory (PDB code 1paz; Petratos et al., 1988). This peptide lies at the junction of a strand of β-sheet and the short loop containing the copper ligands and may reflect strain at that position. The estimated average error from the Luzzati plot for the final native and P80A models is below 0.1 Å. The estimated average error for the oxidized P80I model is slightly above 0.10 Å, and the estimated average error for the reduced P80I model is close to 0.13 Å. The estimated average error in the coordinates, the average esd, and the goodness of fit (Table 3) are correlated with the resolution of the models. For comparisons between models, estimated errors in the difference in position of the average light atom were calculated using the displacement parameter weighted coordinate comparison (DPWCC) method (Libeu & Adman, 1997). These values are 0.11 Å between oxidized and reduced native models, 0.13 Å between P80A models, and 0.15 Å between P80I models, which compare very well with the values calculated from the esd's of 0.13, 0.15, and 0.21 Å, respectively. The relatively higher disagreement for the P80I comparison results from using all pairs of atoms with displacement parameters less than 60 Å^2, whereas DPWCC uses an even more restricted set.

(H) Calculation of the Electrostatic Interactions of the Copper Center. The solvation energies for each of the six models were calculated using the program POLARIS (Lee et al., 1993) which uses the protein dipole−Langevin dipole method to model bulk solvent by a grid of Langevin dipoles near the protein. Details of the choice of parameters required for use of this program are given in Supporting Information.

RESULTS

(A) Mutant Properties. Although ten mutants of pseudoazurin were constructed to explore the environment of the copper center, five (N9P, D37V, R114L, C78S, and G93stop) were not expressed in detectable amounts (Nishiyama, unpublished results). Five exhibited diminished ability to inactivate the electron transfer partner, nitrite reductase: T79V, N41D, M16F, P80A, and P80I. The increased redox potential of the last two, to 409 and 450 mV, respectively, from 270 mV, is likely responsible for the decrease in activity. Previous work has shown that the k_{cat} of nitrite reductase when reduced with P80A was reduced to 0.072 s^{-1} from 0.195 s^{-1} of the wild type whereas the K_m was increased only slightly [10.4 μM from 8.9 μM (Nishiyama et al., 1992)].

(B) Structural Results. *(1) Vector Difference Maps*. The most direct visualization of the structural differences between oxidation states is a vector difference map, shown in Figure 2 for native, P80A, and P80I. In all three maps, the largest peaks lie within 5 Å and are centered on the Cu atom. The next largest peaks are the shift peaks, pairs of positive and negative peaks that indicate an atom has moved, for Pro 35 and Met 7, more than 7 Å from the Cu. This pattern of difference peaks occurs whether the phases for both oxidation states or only the oxidized phases are used in the calculation. The final models for each oxidized and reduced pair are also shown.

Each pseudoazurin exhibits a distinct pattern of difference peaks upon reduction. The ring of negative density around the Cu in the native pseudoazurin map is indicative of an increase in displacement parameter of the Cu and small shifts in position of the Cu and the S^{γ} of Cys 78. The pattern for the mutants is quite different. The shift peaks for P80A pseudoazurin are consistent with a movement of the Cu closer to the plane formed by the S^{γ} of Cys 78, $N^{\delta 1}$ of His 40 , and $N^{\delta 1}$ of His 81 upon reduction. There is also a significant shift peak for the S^{δ} of Met 86. Although the magnitudes of the peaks are much smaller, the shift peaks in the vector difference map for oxidized and reduced P80I follow the same pattern as the shift density in the P80A vector difference map.

(2) Bond Angles and Distances. Table 4 shows the bond distances and angles at the copper for the pseudoazurin models. Bond lengths from models refined with SHELXL are systematically shorter than bond lengths for models refined with either PROLSQ or X-PLOR (all models in the table shown with no estimated standard deviations). This effect was noticed during the early stages of the SHELXL refinement and coincided with the first cycle in which the displacement parameters of the Cu and the sulfurs were refined anisotropically. However, the effect is small enough that oxidized native ligand bond lengths are not significantly different from ligand bond lengths in the previously published oxidized native model (PDB code 1paz; Petratos et al., 1988). The ligand bond lengths are not significantly different for any of the high pH reduced and oxidized pairs, except for a lengthening of the methionine bond length upon reduction in the native and P80A mutant pseudoazurin.

Significant differences are observed in the bond angles for each of the pairs. In native pseudoazurin, the $N^{\delta 1}$ 40−Cu−S^{γ} 78 angle significantly increases (10° ± 1°), and the $N^{\delta 1}$ 81−Cu−S^{γ} 78 angle significantly decreases (−7° ± 1°) upon reduction, consistent with the shift peak for S^{γ} 78 in

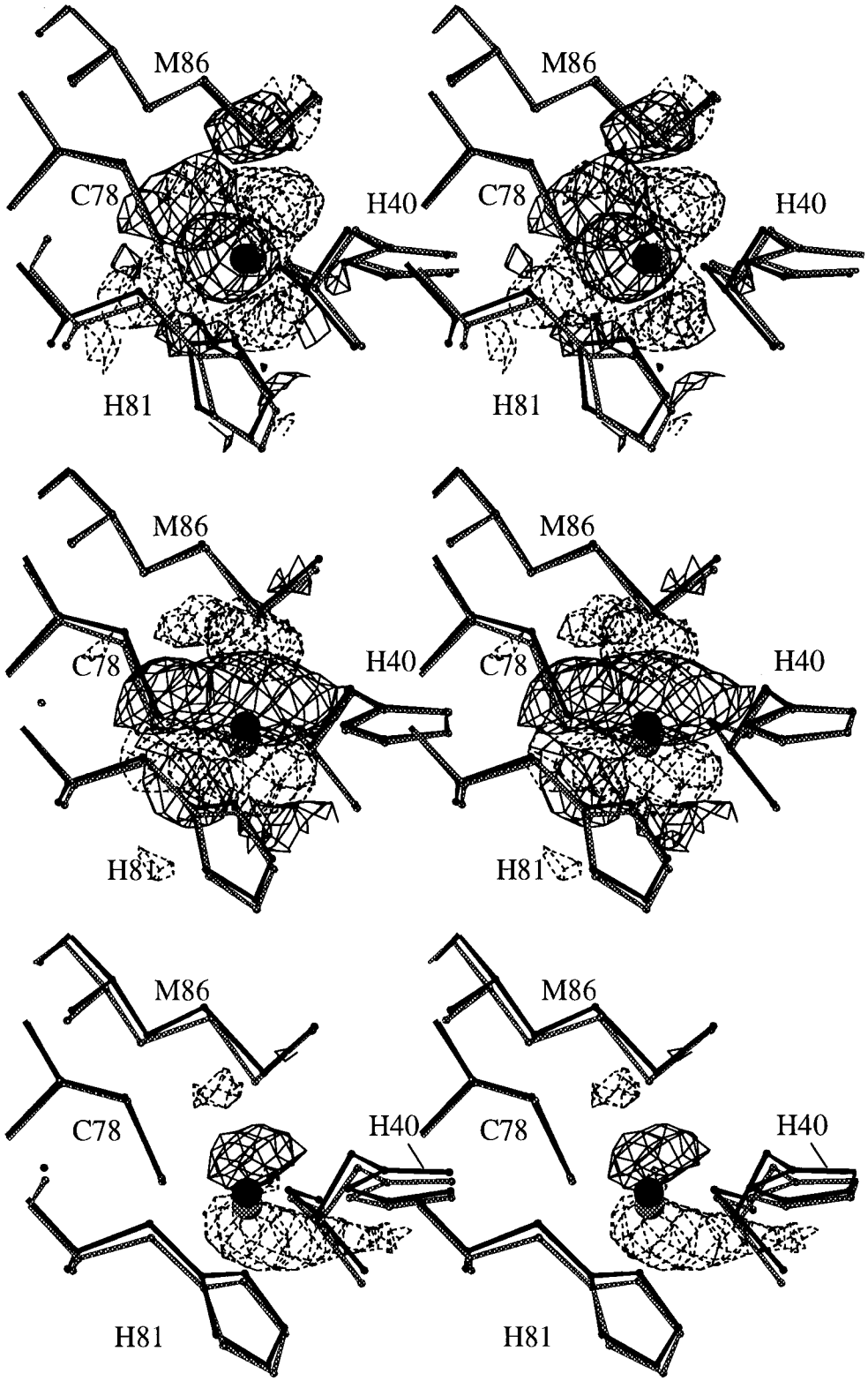

FIGURE 2: Vector difference maps for each pseudoazurin: native (top), P80A (middle), and P80I (bottom). The maps are contoured at $+3.5\sigma$ (solid) and -3.5σ (dotted). The Fourier vector difference maps are calculated with the phases from the refinement and the observed magnitudes of the structure factors. $\Delta\rho(x,y,z) = \sum(F_{o,ox}(hkl)e^{-2\pi i\alpha_{ox}(hkl)} - F_{o,red}(hkl)e^{-2\pi i\alpha_{red}(hkl)})e^{-2\pi i\mathbf{HX}}$. $F_{o,ox/red}(hkl)$ is the observed magnitude of the structure factor of the oxidized or reduced form, $\alpha(hkl)$ is the calculated phase for the oxidized or reduced form, and **HX** is the dot product of the reciprocal space vector with the real space vector. The appropriate oxidized model is drawn in black, and the reduced model is shown in gray. The Cu is represented by a sphere. σ is 0.49 e/Å^3 for native pseudoazurin, 0.51 e/Å^3 for P80A pseudoazurin, and 0.35 e/Å^3 for P80I pseudoazurin.

the vector difference map for native pseudoazurin. In P80A pseudoazurin, $N^{\delta 1}$ 81−Cu−S^{γ} 78 significantly *increases* (8° ± 1°) upon reduction, while $N^{\delta 1}$ 81−Cu−S^{δ} 86 decreases. The only significant difference in bond angles between the oxidized and reduced P80I pseudoazurin is an increase of 7° in S^{γ} 78−Cu−S^{δ} 86, consistent with the vector difference map (Figure 2).

(3) Changes in the Coordination of the Copper. The subtle changes in the geometry of the copper center can be better examined by comparing the variation of the perpendicular distances between the Cu and a plane formed by three of the ligands. There are four unique planes defined by

Table 4: Bond Lengths and Angles for Pseudoazurin[a]

	H40	C78	H81	M86	H40−C78	H40−H81	H40−M86	C78−H81	C78−M86	H81−M86
oxidized native[b]	2.16	2.16	2.12	2.76	136	100	87	112	108	112
oxidized native	2.01 (3)	2.13 (2)	2.01 (3)	2.71 (2)	133 (1)	100 (1)	89 (1)	113 (1)	106.8 (5)	111 (1)
red native, pH = 7.8[c]	2.16	2.16	2.28	2.90	140	102	85	108	107	110
red native, pH = 7.0	2.10 (4)	2.16 (2)	2.31 (5)	2.81 (3)	143 (1)	98 (2)	88 (1)	106 (1)	108.5 (8)	111 (1)
oxidized P80A	1.98 (4)	2.14 (2)	1.95 (4)	2.76 (2)	135 (1)	103 (2)	88 (1)	110 (1)	107.6 (7)	110 (1)
reduced P80A	2.05 (4)	2.18 (2)	2.02 (4)	3.00 (2)	136 (2)	102 (2)	82 (1)	118 (1)	105.6 (7)	100 (1)
oxidized P80I	2.01 (5)	2.13 (3)	2.07 (5)	2.90 (3)	135 (2)	98 (2)	85 (1)	118 (2)	108 (1)	107 (2)
reduced P80I	2.04 (7)	2.14 (4)	2.12 (7)	2.95 (5)	138 (3)	96 (3)	85 (2)	121 (3)	101 (2)	103 (2)
oxidized K10DK38D[d]	2.11	2.15	2.05	2.77	136	102	86	113	106	109
oxidized K38D[d]	2.05	2.10	2.07	2.67	136	99	88	112	108	110

[a] Bond lengths (Å) are given in first four columns and bond angles (deg) in next six. Standard uncertainties are given in parentheses where derived from SHELXL refinement in which estimates of standard uncertainties in atom positions are generated from full-matrix restrained least squares. [b] Pseudoazurin model (1paz; Petratos et al., 1988). [c] Pseudoazurin model (1pza; Vakoufari et al., 1994). [d] Kukimoto et al., 1995.

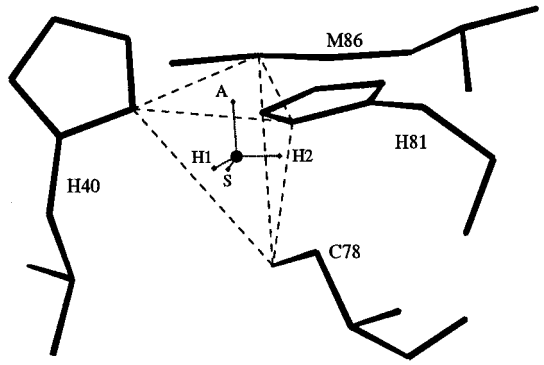

FIGURE 3: Definition of the ligand planes. Each ligand plane is formed by three of the ligands: the plane of the strong ligands (S) by $N^{\delta 1}$ of His 40, $N^{\delta 1}$ of His 81, and S^{γ} of Cys 78, the accessible plane (A) by $N^{\delta 1}$ of His 40, $N^{\delta 1}$ of His 81, and S^{δ} of Met 86, the His 40 plane (H1) by $N^{\delta 1}$ of His 40, S^{δ} of Met 86, and S^{γ} of Cys 78, and the His 81 plane (H2) by $N^{\delta 1}$ of His 40, S^{δ} of Met 86, and S^{γ} of Cys 78. The sphere marks the position of the Cu. The dotted lines show the distance between the copper and each plane.

permutations of combinations of the ligand atoms (Figure 3). These planes represent faces of the distorted tetrahedron formed by connecting all copper ligand atoms. In perfect tetrahedral coordination, the copper would lie at the center of the tetrahedron; e.g., it would be equidistant from each of the coordinate planes. The pattern of these distances describes the degree of distortion from tetrahedral geometry of the copper with only four parameters. Table 5 shows the perpendicular distance between the Cu and each of the planes determined by the ligands, in the present structures and other cupredoxins.

In each of the oxidized cupredoxins, the same pattern of distorted tetrahedral geometry is observed. The copper is much further from the plane composed of the more solvent-accessible ligands (A) than the other three planes. Except in *Methylobacterium extorquens* pseudoazurin, the distances between the copper and the planes with the two strong ligands (H1 and H2) are almost equivalent. These distances disagree by no more than 0.10 Å, well within the magnitude of the estimated errors. The pseudosymmetry between these planes is seen spectroscopically for plastocyanin using EXAFS and EPR (Gray et al., 1981).

The distance between the copper and the plane determined by the three strong ligands (S) has been predicted to shorten upon reduction in pseudoazurins (Solomon, 1983), forming the strongest possible trigonal copper coordination. In P80A and P80I pseudoazurin this distance shortens by 0.16 ± 0.03 Å and 0.13 ± 0.05 Å upon reduction. The distance is also shorter in the oxidized P80A and P80I models, with 0.43 ± 0.02 Å for native, 0.39 ± 0.02 Å for P80A, and 0.35 ± 0.03 Å for P80I pseudoazurin. Although the resolution is too low for confident prediction, the increase in redox potential of the P80A and P80I pseudoazurin is inversely correlated with the length of the normal distance between the copper and the plane of the three strong ligands.

This correlation is consistent with the hypothesis that the more trigonal in character the oxidized copper center, the higher the redox potential of the protein (Fee & Malmström, 1968), but other factors override when dissimilar cupredoxins are compared. For example, in *Alcaligenes denitrificans* azurin the normal distance to the plane determined by the three strong ligands is even smaller than P80I pseudoazurin, but the redox potential is nearly identical to native pseudoazurin (Sykes, 1990). Unlike the mutant pseudoazurins, the distance to the plane of the three strong ligands does not change appreciably upon reduction. However, the coordination sphere of the copper in *A. denitrificans* azurin contains an extra carbonyl oxygen not found in the plastocyanin-like pseudoazurins.

(4) Change in Displacement Parameters upon Reduction. (a) Isotropic Displacement Parameters. The displacement parameters are systematically higher in reduced pseudoazurins than in oxidized pseudoazurins. The increase in mean displacement parameter upon reduction is 6 $Å^2$ for native pseudoazurin, 2 $Å^2$ for P80A pseudoazurin, and 6 $Å^2$ for P80I pseudoazurin. The mean displacement parameter of oxidized P80I pseudoazurin is also 5 $Å^2$ higher than the mean displacement parameter of oxidized native pseudoazurin. The pseudoazurins with more trigonal copper centers appear to have overall higher displacement parameters. However, comparison between the P80I pseudoazurins and the native or P80A pseudoazurins is difficult because the P80I pseudoazurin crystals have a slightly different crystal form. P80I crystals have a slightly larger cell edge perpendicular to the 6-fold axis (50.79 Å versus 50.06 Å) and a slightly shorter cell edge parallel to the 6-fold axis (98.25 Å versus 98.79 Å). The crystal contacts are identical between the two forms except for the participation of the Ile 80 side chain in one of the contacts. Such a small increase in average displacement parameter as 5 $Å^2$ cannot be confidently ascribed solely to the increased trigonality of the copper center in oxidized P80I.

The *pattern* of change in the displacement parameters upon reduction for the three pseudoazurins is very different (Figure 4). In native pseudoazurin, the increase in the displacement parameters is fairly evenly distributed through the molecule, and there are relatively few very large changes in the displacement parameters. In P80A pseudoazurin, the large

Table 5: Distance between Cu and Ligand Triad Planes[a]

	PDB code	S	A	H1	H2
A. faecalis pseudoazurin ox native[b]	1paz	0.43	1.08	0.67	0.73
A. faecalis pseudoazurin ox native	8paz	0.43 (2)	1.01 (2)	0.69 (2)	0.71 (2)
A. faecalis red native, pH = 7.8[b]	1pza	0.37	1.13	0.63	0.84
A. faecalis red native, pH = 7.0	3paz	0.43 (2)	1.12 (3)	0.54 (3)	0.84 (2)
A. faecalis red native, pH = 5.5[c]		0.79	1.19	0.22	0.78
A. faecalis red native, pH = 4.5[b]	1pzb	0.77	1.09	0.22	0.87
A. faecalis ox P80A	4paz	0.39 (2)	1.00 (3)	0.65 (2)	0.76 (2)
A. faecalis red P80A	5paz	0.23 (2)	1.16 (3)	0.71 (2)	0.81 (2)
A. faecalis ox P80I	6paz	0.35 (3)	1.13 (3)	0.68 (3)	0.72 (3)
A. faecalis red P80I	7paz	0.22 (4)	1.20 (5)	0.69 (4)	0.79 (4)
A. faecalis ox K10DK38D[c]		0.41	1.05	0.63	0.72
A. faecalis ox K38D[c]		0.36	1.07	0.69	0.76
M. extorquens pseudoazurin ox native[d]	1pmy	0.39	1.08	0.53	0.71
P. nigra plastocyanin ox, 1.6 Å[e]	1pnc	0.34	1.18	0.72	0.69
P. nigra plastocyanin ox, 1.33 Å[e]	1plc	0.36	1.13	0.65	0.70
P. nigra plastocyanin red, pH = 7.8[e]	4pcy	0.46	1.25	0.48	0.80
P. nigra plastocyanin red, pH = 7.0[e]	5pcy	0.47	1.19	0.59	0.80
P. nigra plastocyanin red, pH = 3.8[e]	6pcy	0.70	1.39	0.10	1.04
E. prolifera plastocyanin ox[f]	7pcy	0.38	1.06	0.75	0.74
C. reinhardtii plasticyanin ox[g]	2plt	0.31	1.13	0.72	0.73
P. denitrificans amicyanin ox[h]	1aac	0.30	1.02	0.67	0.83
cucumber stellacyanin ox[i]	1jer	0.33	1.00	0.67	0.78
T. ferrooxidans rusticyanin ox[j]	1rcy	0.33	1.02	0.82	0.72
A. denitrificans azurin ox[k]	2aza	0.13 (4)			
A. denitrificans azurin reduced[k]		0.14 (2)			

[a] Numbers in parentheses are standard deviations derived from standard uncertainties in atomic positions from SHELXL refinement; unreferenced entries are this work. S, A, H1, and H2 are defined in Figure 3. [b] Pseudoazurin models (1paz, Petratos et al., 1988; 1pza, Vakoufari et al., 1994). [c] Kukimoto et al., 1995. [d] *Methylobacterium extorquens* pseudoazurin (Inoue et al., 1994). [e] *Populus nigra* plastocyanin (Guss et al., 1986). [f] *Enteromorpha prolifera* plastocyanin (Collyer et al., 1990). [g] *Chlamydomas reinhardtii* plastocyanin (Redinbo et al., 1993). [h] *Paracoccus denitrificans* amicyanin (Durley et al., 1993). [i] Cucumber stellacyanin (Hart et al., 1996). [j] *Thiobacillus ferrooxidans* rusticyanin (Walter et al., 1996). [k] *Alcaligenes denitrificans* azurin (Baker, 1988; Shepard et al., 1990) (data from publication; coordinates for reduced form not deposited in Protein Data Bank).

increases in displacement parameters are found in the surface side chains, while the main chain atoms and side chain atoms within the β-barrel tend to exhibit relatively small changes. The pattern for P80I pseudoazurin is very similar to the native, except that there are more side chains with a relatively large increase in displacement parameters. In addition, for P80I, there is a noticeable decrease in the change in the displacement parameters for residues in the ligand loop between 78 and 86. The change in the displacement parameters decreases for the *main* chain atoms of Tyr 82, Met 84, and Ile 80 (not shown) and for some of the side chain atoms of Ile 80. For the remaining side chain atoms, the increase in displacement parameter upon reduction is smaller than the mean change overall. In contrast, the displacement parameters of the side chains of both Pro 80 in native pseudoazurin and Ala 80 in P80A pseudoazurin increase by more than the mean overall change. The side chain of Met 84 also shows smaller changes in the displacement parameters for P80I pseudoazurin than for either P80A or native pseudoazurin. The apparent rigidity of Ile 80 may be due to the altered hydrogen-bonding network discussed later or its participation in the crystal contact. The lowered mobility of Met 84 may result from a $\sigma-\pi$ interaction with His 81. Whatever the mechanism, the displacement parameters of the triligand loop only show a consistent increase upon reduction in native pseudoazurin.

(b) Anisotropic Displacement Parameters. The copper and sulfur atoms were refined anisotropically in each pseudoazurin. The relative anisotropy of each atom is related to the vibrational motion of the atoms and the degree of disorder in the copper site. Figure 5 shows the thermal ellipsoids for the copper and the sulfur ligands contoured at the 50% probability level. Normal mode analysis of model compounds of the reduced copper site indicates that the lowest order motions in the copper site should be bending motions (Gluckert et al., 1995). If anisotropy of the copper and sulfur atoms reflects these motions, the long axis of the sulfur atom thermal ellipsoids should be perpendicular to the bonds. In each pseudoazurin, the long axis of the thermal ellipsoids of the Cys S^{γ} of the cysteine is nearly perpendicular to the Cu−Cys bond, consistent with harmonic motion of the sulfur due to bending modes. However, the long axis of the thermal ellipsoids of Met S^{δ} is very nearly parallel to the Cu−S^{δ} bond in all the pseudoazurins. This orientation indicates that a multiple population of copper centers may be present in each crystal with slightly varying Cu−S^{δ} bond lengths.

(5) Changes in Packing near the Site of the Mutation. The gross orientation of the ligand planes is due to tight packing of ligand residues. All the side chains participate in a network of hydrogen bonds and have extensive van der Waals contacts with atoms in their own loops and adjacent loops. His 81 has the least extensive van der Waals contacts. All ring atoms except $N^{\delta 1}$ of His 81 contribute to the solvent-accessible surface in all six forms of pseudoazurin. The backbone of His 81 is tightly packed between Pro 80 and Phe 82. Mutation of Pro 80 has only very local effects in both mutants and primarily alters the packing and solvent accessibility of His 81 while leaving other ligands undisturbed.

As shown in Figure 6, mutation of Pro 80 directly affects solvent accessibility of the backbone of His 81. In P80A, removal of the proline side chain creates a small pocket, which is filled by a new water molecule unique to the P80A mutant. This pocket is lined by atoms from Gly 39, Asn 41, Thr 79, and Ala 80. The contribution of each of these residues to the molecular surface increases except for Asn 41, which is the most buried of the group. The water molecule makes hydrogen bonds with the amide nitrogen of Ala 80, $O^{\delta 1}$ of Asn 41, and the carbonyl oxygen of Gly 39 (not shown). The C^{α} and C^{β} atoms of P/A 80 are also

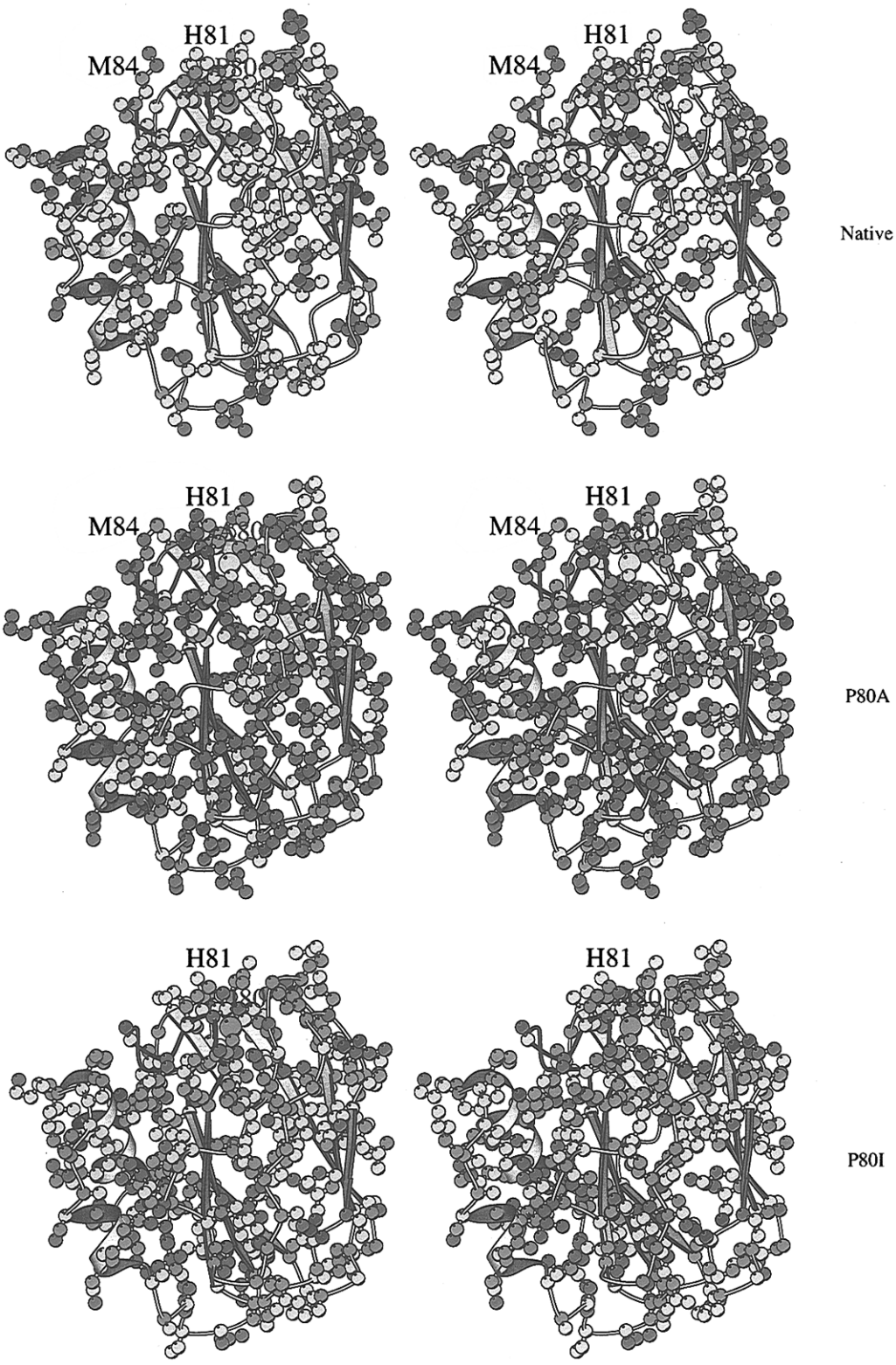

FIGURE 4: Difference in displacement parameters between oxidized and reduced pseudoazurins: native (top), P80A (middle), and P80I (bottom). Only side chains with an atom whose absolute value of the difference in displacement parameters is greater than the mean difference in displacement parameters (m) for the comparison are shown. The atoms are colored so that red is a difference in displacement parameter greater than $2m$, orange is between m and $2m$, yellow is between 0 and m, green is between $-m$ and 0, blue is between $-2m$ and $-m$, and purple is less than $-2m$. The backbone of the triligand loop is drawn in black. The mean and the variance (in Å^2) of the displacement parameters for protein atoms in each coordinate set are as follows: native, oxidized 23 ± 14 and reduced 28 ± 17; P80A, oxidized 23 ± 13 and reduced 25 ± 13; P80I, oxidized 27 ± 11 and reduced 33 ± 12.

significantly shifted, so that the side chain of the alanine packs against the side chain of His 81. This shift in position is most likely due to both less restricted ϕ, ψ angles for alanine and to the new water molecule that replaces C$^\beta$ and C$^\gamma$ of the proline side chain. The vector difference density for the P80A mutation (Figure 7) shows that while the peptide 79−80 that contains the amide nitrogen predicted to form a new NH−S hydrogen bond rotates slightly in the right direction, the new water competes for this hydrogen.

The differences between P80I and native pseudoazurin at the mutation site are also very small. The most affected atoms other than the copper are C$^\beta$ and C$^\gamma$ of the P/I side

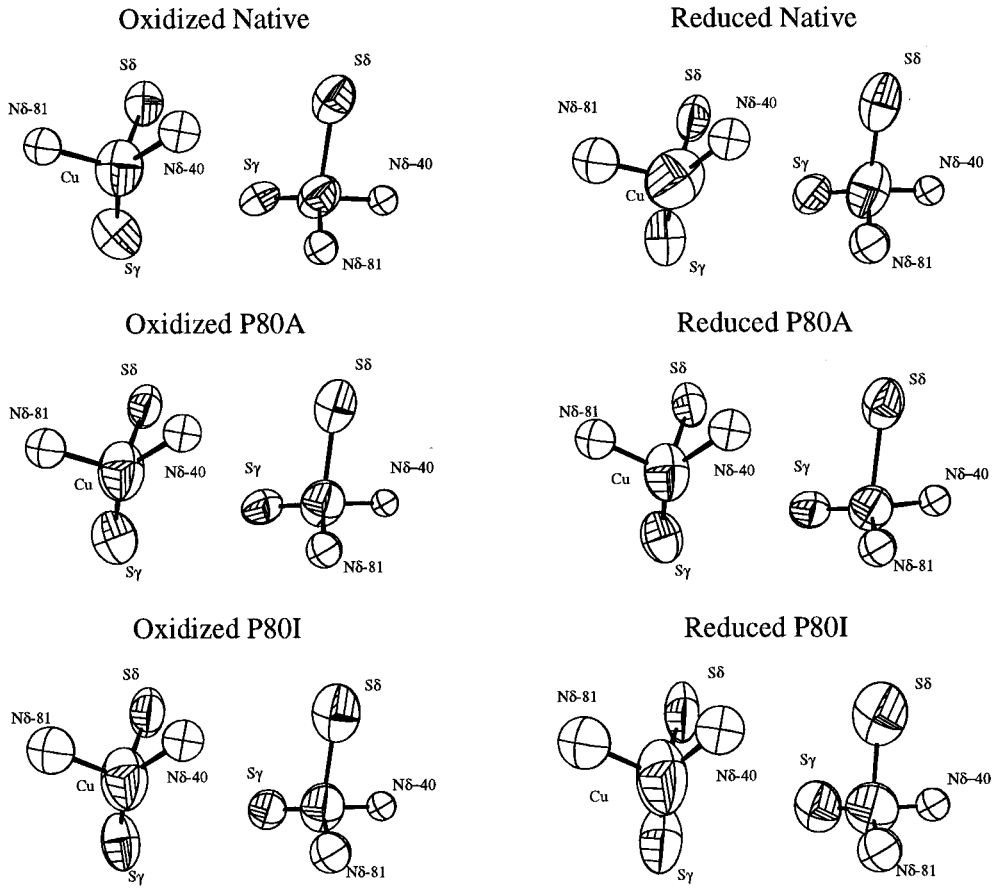

FIGURE 5: Anisotropic displacement parameters for the copper and sulfur ligands in pseudoazurin. All thermal ellipsoids are drawn at 50% probability. The nitrogens were not refined anisotropically. The left member of each pair is viewed normal to the strong ligand plane (C, H1, H2) while the right is viewed with the S−Cu−H1 plane horizontal.

chain as well as atoms from Ile 60 and Gly 39 that pack against the new isoleucine side chain. The carbonyl of Gly 39 is the only atom to make a van der Waals contact with the side chain of Ile 80. Extension of Ile 80 into the space occupied by Ile 60 is accommodated by altered mobility of the Ile 60. In native and P80A pseudoazurin, Ile 60 has two conformations. One of the conformations conflicts with Ile 80 and is not observed in the P80I difference maps. Although introduction of the isoleucine partially buries His 81, as the $C^{\gamma 1}$ packs over the histidine ring, the conformation of His 81 is not significantly different between native and P80I pseudoazurin.

(6) Changes in the Pattern of Hydrogen Bonding. In addition to van der Waals interactions, the orientation of the ligands is also stabilized by several hydrogen bonds. These hydrogen bonds occur either within the triligand loop (the loop that contains the Cys, His, and Met), between the loops, or with water (Table 6). The backbone atoms of Cys 78, His 81, and Met 86 form a ring of buried hydrogen bonds: O C78−N H81, O H81−N M86, and O M86−N C78 (Figure 8). Together these hydrogen bonds are a powerful constraint on the conformations the three ligands can adopt. Hydrogen bonds between Thr 79 and Asn 41 link the two ligand-containing loops. The hydrogen bonds between Gly 39 and Asn 61 link ligand- and nonligand-containing loops and reinforce the van der Waals interactions among the four loops that surround the copper site. Within all six models, hydrogen bonds between the ligand-containing and nonligand-containing loops as well as those involving residues around His 40 are constant, while hydrogen bonds within the triligand loop, between Thr 79 and Asn 41 or to water molecules, vary upon oxidation state change.

In both native and P80A pseudoazurin, the weak O C78−N H81 hydrogen bond loosens upon reduction. The analogous hydrogen bond is broken in reduced pH 7.0 poplar plastocyanin (Guss et al., 1986). Similarly, the O H81−N M86 hydrogen bond lengthens slightly in both reduced pseudoazurin and reduced poplar plastocyanin. The lengthening (breaking) of both these hydrogen bonds may act to relieve strain in the triligand loop associated with a subtle expansion of the Cu site.

The pair of bonds between Asn 41 and Thr 79 changes differently for P80A and P80I. In the native structure, $N^{\delta 2}$ 41−$O^{\gamma 1}$ 79 stays the same, while $O^{\delta 1}$ 41−N 79 decreases. In P80A both decrease; in P80I both increase. This may be linked to the hydrogen bond between $O^{\gamma 1}$ 79 and $O^{\epsilon 2}$ 43, which increases in native and P80A but decreases in P80I. These changes reflect slightly different packing around the side chain of residue 80.

Reduction of P80A pseudoazurin moves the new water molecule closer to the surface of the small cleft. This small movement breaks the weak hydrogen with the amide of Ala 80, so that the water molecule makes only a single hydrogen bond with $O^{\delta 1}$ of Asn 41.

(7) Changes in the Pattern of Hydration of the Copper Site. Apart from the new water, the first-shell water models for the oxidized and reduced pseudoazurins are almost identical even though they were determined independently. (Water molecules are considered identical if they are no more than 0.25 Å apart in the reduced and oxidized models and at least one hydrogen bond is conserved.) All of the second-shell water molecules are found in a majority of the six

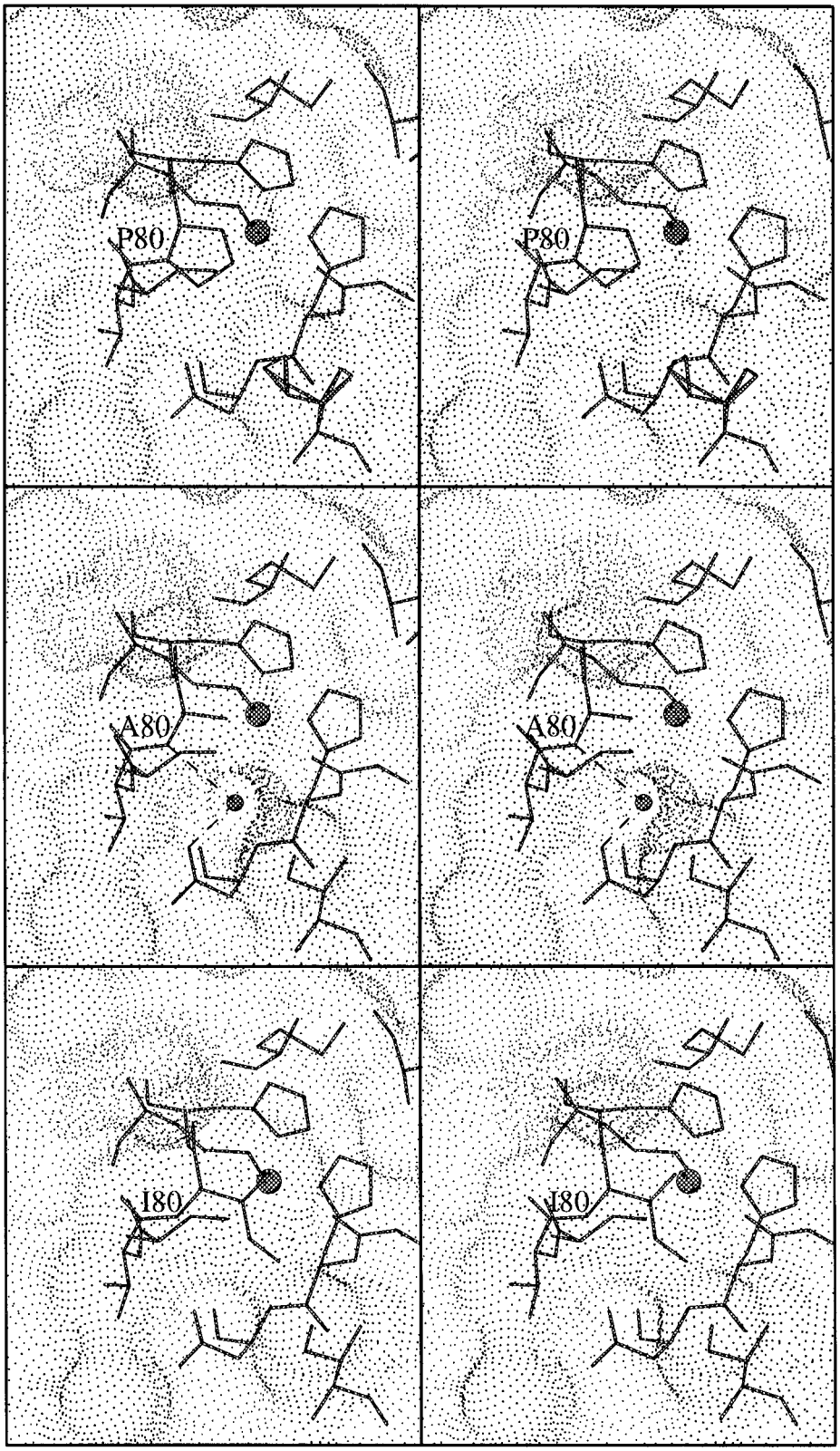

FIGURE 6: Accessible surface near the mutation site for native, P80A, and P80I pseudoazurin. The accessible surface was calculated with the MS program (Connolly, 1983) using an 1.4 Å probe radius. The large sphere is the copper, while the small spheres are water molecules. (Ile 60 is in the lower right of the figure.)

structures, and there are no unfilled second-shell water positions that do not have residual density in the final ($F_o - F_c$) Fourier difference maps. The absences are most likely a result of varying resolutions and data quality rather than true differences between the models. Besides the new water(Wat 218) the unique first-shell water molecules are Wat 402 that forms a hydrogen bond with the amide nitrogen of His 40 in oxidized native pseudoazurin and Wat 275 that forms a hydrogen bond with the carbonyl oxygen of Ala 80 in reduced P80A pseudoazurin. In addition, in all five models except reduced P80I, a water molecule is bound to the $N^{\epsilon 1}$ of His 81. No residual density is present at the site of this water in the final ($F_o - F_c$) Fourier difference map of reduced P80I pseudoazurin. In reduced P80A pseudoazurin, the hydrogen bond between this water molecule and $N^{\epsilon 1}$ of His 81 is 0.16 Å longer than in the oxidized P80A,

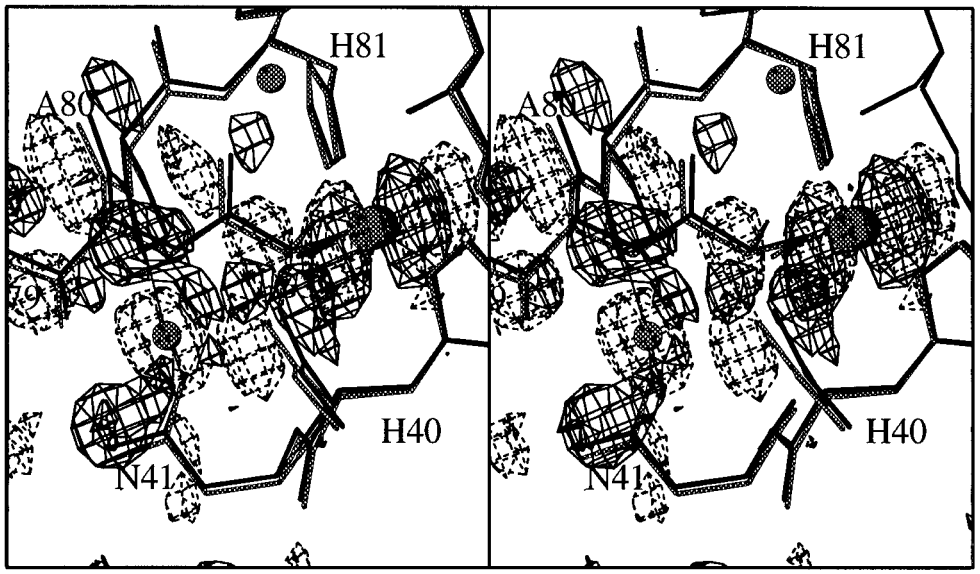

FIGURE 7: Vector difference density of oxidized native minus oxidized P80A at the site of the new water in the cleft of P80A. The maps are contoured at $+4.0\sigma$ (solid) and -4.0σ (dotted). The model of oxidized P80A is also shown in black, and the oxidized native model is shown in gray. σ is 0.42 e/Å^3. The large sphere is the copper atom, while the small spheres are the new water and the water bonded to His 81. Shift peaks resulting from reorientation of peptide 79/80 as well as peptide 39/40 are easily visible.

Table 6: Possible Hydrogen Bonds within 5.0 Å of Copper in Pseudoazurins[a]

		oxidized native	reduced native	oxidized P80A	reduced P80A	oxidized P80I	reduced P80I
intraprotein hydrogen bonds							
N G39	$O^{\delta 1}$ N61	2.68	2.71	2.61	2.62	2.60	2.61
O H40	N N61	2.91	2.92	2.97	3.05	2.92	2.79
$N^{\epsilon 2}$ H40	$O^{\delta 1}$ N9	(**2.76**	**2.84**)	(**2.72**	**2.86**)	[**2.88**	**2.77**]
$O^{\delta 1}$ N41	N T79	[**2.82**	**2.73**]	[**2.86**	**2.75**]	(**2.76**	**2.88**)
$N^{\delta 2}$ N41	$O^{\gamma 1}$ T79	3.06	3.05	[**3.10**	**2.92**]	(**2.90**	**3.15**)
	O S58	3.12	3.03	3.06	3.11		3.23
N C78	O M86	(**3.02**	**3.10**)	(**3.12**	**3.20**)	3.15	3.15
O C78	N H81	**3.15**		**3.29**		3.24	3.22
$O^{\gamma 1}$ T79	$O^{\epsilon 2}$ E43	(**2.42**	**2.56**)	(**2.60**	**2.75**)	[**2.60**	**2.50**]
O H81	N M86	3.16	3.20	(**3.15**	**3.25**)	**3.26**	
	N M84	[**3.03**	**2.92**]	(**2.93**	**2.92**)	[**3.03**	**2.86**]
N (80)	S^{γ} C78	4.05	3.86	[**3.66**	**3.46**]	[**3.64**	**3.53**]
N N41	S^{γ} C78	3.58	3.70	3.70	3.65	3.59	3.53
hydrogen bonds with water							
N 40	O W402	**2.89**	–	–	–	–	–
$O^{\delta 1}$ N41	O W218	–	–	(**2.75**	**2.84**)	–	–
O T79	O W203	(**2.86**	**2.94**)	(**2.94**	**2.91**)	(**2.84**	**3.01**)
N A80	O W218	–	–	**3.24**		–	–
O A80	O W275	–	–	–	2.90	–	–
$N^{\epsilon 2}$ H81	O W216	2.79	2.79	(**2.76**	**2.92**)	**2.72**	

[a] O and N distances <3.4 Å are listed. A dash means that there is no solvent molecule at that position. Pairs of distances in boldface indicate possibly significant trends: values enclosed in brackets are decreases, and values enclosed in parentheses are increases.

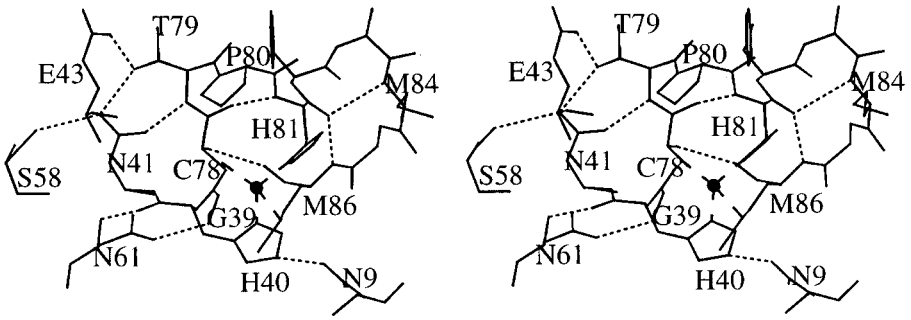

FIGURE 8: Hydrogen bonds within 5 Å of the copper atom in pseudoazurin. The hydrogen bonds are depicted with dotted lines, while the ligand copper bonds are depicted with dashed lines. The bond lengths for all six pseudoazurins are listed in Table 6. The oxidized native pseudoazurin model was used to draw this picture.

consistent with the loss of the water in the reduced P80I model. Similar changes in first-shell water models are also observed between native and pH 7.0 reduced plastocyanin. In plastocyanin, the carbonyl oxygens of Pro 86 and Ser 85 only form hydrogen bonds with water molecules in the reduced pH 7.0 plastocyanin structure (Guss et al., 1986).

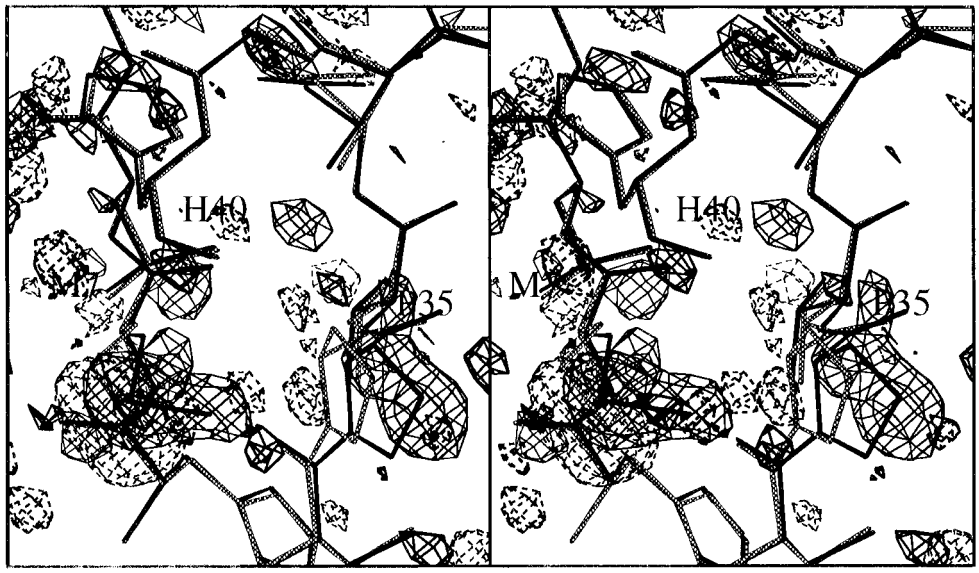

FIGURE 9: Vector difference map (oxidized − reduced) at Met 7/Pro 35 for native pseudoazurin. The maps are contoured as in Figure 2. The oxidized model is shown in black, and the reduced model is shown in gray. The pair of negative (dashed) and positive (solid) peaks at the lower left belong to Met 7 and, unfortunately, must be viewed nearly along the extension of the side chain from the viewer into the paper. The shift itself is left to right in the plane of the paper.

These differences in hydration between the oxidized and reduced forms may reflect subtle changes of the electrostatics of the copper center, since each water molecule lost or gained represents a small shift in the dipole term of the electrostatic potential at the copper center.

(8) Changes in the Loop Containing His 40. Unlike the other ligands, the orientation of His 40 is primarily controlled by a strong hydrogen bond between His 40 $N^{\epsilon 2}$ and $O^{\delta 1}$ of Asn 9 (one of the mutants attempted was N9P, but it was not expressed). At pH 7.0, this hydrogen bond is conserved in both oxidation states of the mutant and native pseudoazurins. Similarly, the hydrogen bonds between the amide nitrogen of Gly 39 and $O^{\gamma 1}$ of Asn 61 and between the carbonyl oxygen of His 40 and the amide nitrogen of Asn 61 are preserved in all six models. The loss of Wat 402 from the amide nitrogen of His 40 after reduction in native pseudoazurin is most likely related to subtle changes of packing of the loop containing His 40. The only major site of difference electron density outside the copper center in the vector difference Fourier maps between each pair of oxidized and reduced structures is directly behind His 40 (Figure 9). In the oxidized pseudoazurins, S^{δ} of Met 7 packs against C^{β} of His 40. In each reduced pseudoazurin, a small shift of the side chain of Met 7 moves the less electron dense C^{ϵ} into the approximate position of S^{δ} and makes an additional van der Waals contact with the carbonyl carbon of His 40. In each pseudoazurin, the displacement of Met 7 is coupled to a change in the position of Pro 35 which in turn causes the loss of Wat 402 upon reduction in native pseudoazurin. The new position of C^{β} of Pro 35 partially occludes the water site in reduced native pseudoazurin. The differences are seen in all three forms and are mostly likely directly coupled to the change in geometry of the copper center.

All of the large differences between each pair of oxidized and reduced pseudoazurins are shown in Figure 10; those at the surface of the molecule and associated with mobile or poorly determined side chains common to all the models are far from the copper atom and are not shown. Near the copper atom are the significant change in Met 7 and Pro 35 described above, smaller shifts in His 81, Met 84, and Met 86, and significant changes at Cys 78 and a small shift in Phe 18 for both native and P80A pseudoazurin. Most of these differences are also seen when the oxidized models are compared (Figure 11), although the shift in the positions of S^{δ} of Met 7 and Pro 35 is much smaller, consistent with the notion that the mutants favor a reduced structure. Intriguingly, how much Met 7 moves appears to be correlated with the length of the Cu−S^{δ} 86 bond. There also appears to be a relationship between His 81 and Met 84: in all five comparisons, both side chains move so that the distance from the S^{δ} of Met 84 to the center of the histidine ring is preserved.

(9) Role of Weak Electrostatic Interactions. The apparent linkage between Met 7 and the copper center may be mediated by weak electrostatic interactions involving inducible dipoles of the p electrons of the sulfur atoms and the π electrons of aromatic rings. The aromatic ring of Phe 18 is positioned so that it forms a $\sigma-\pi$ interaction with S^{δ} of either Met 86 or Met 7, depending on their relative positions. In addition to the possible interactions with methionines, Phe 18 is also positioned so that the π orbital of the aromatic ring is nearly parallel with the amide dipoles of residues 76, 77, 86, and 87, at the beginning and the end of the triligand loop. [Peptide dipoles (or amide dipoles) lie in the peptide plane running roughly from the carbonyl oxygen to midway between the peptide nitrogen and its hydrogen.] Phe 18 packs against only one other residue, Phe 33, but at an angle of 76°, somewhat less optimal for dipole induction. For a residue completely buried in the core of the β-barrel, Phe 18 is in a surprisingly polarizable environment. None of the other four aromatic residues in pseudoazurin have geometries as favorable to dipole induction through weak electrostatic interactions.

Quantum mechanical calculations in vacuum have estimated that, in the optimal geometry for dipole induction, these weak interactions can be between 3.0−5.0 kcal/mol for amide−aromatic interactions and 1.0−1.5 kcal/mol for sulfur−aromatic interactions (Cheney et al., 1989). The optimal distance for the amide−aromatic interaction is 3.6−

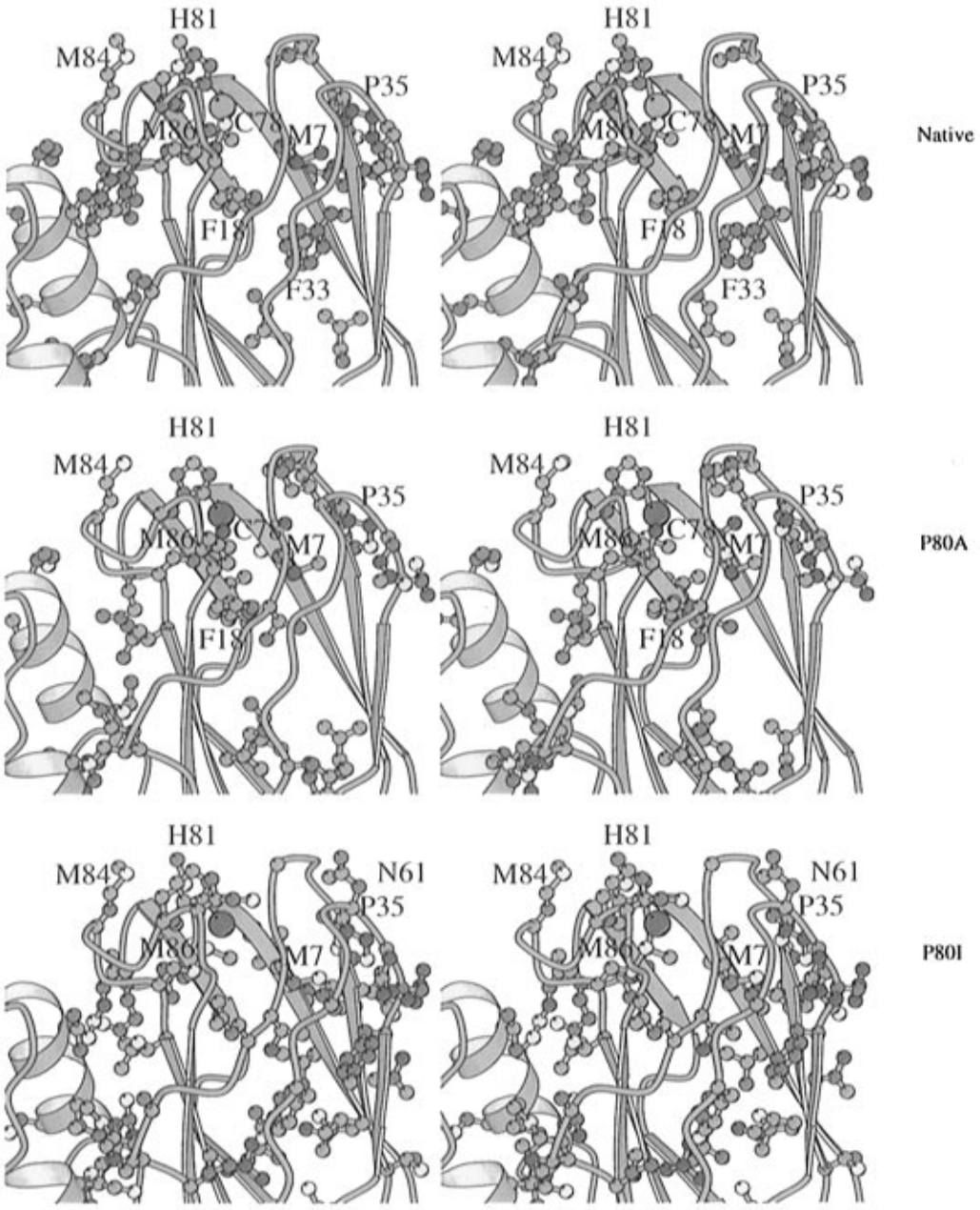

FIGURE 10: Stereoview of the comparison between the oxidized and reduced models of native (top), P80A (middle), and P80I pseudoazurin (bottom). The atoms are colored so that blue is a probability of difference less than 25%, green is between 25% and 50%, yellow is 50−70%, and red is greater than 70%. Only residues that contain at least one atom with a probability of difference greater than 30% are shown. For a definition of the probability of difference, see Libeu and Adman (1997). The disordered surface lysines are not shown.

4.5 Å, with the amide dipole parallel to the normal to the plane of the aromatic ring. The optimal distance for the sulfur aromatic interactions is 4.0−5.0 Å with the p orbital parallel to the normal to the plane of the aromatic ring. Since the difference in redox potential between the mutant and native pseudoazurin is less than 5.0 kcal/mol, formation of favorable weak interactions upon reduction could contribute significantly to the difference in redox potential.

A survey of the weak electrostatic interactions for all six forms of pseudoazurin as well as all the high-resolution cupredoxin structures shows that some of the interactions involving the ligand residues change consistently in response to reduction of the copper site (Tables 7 and 8 and Figure 12). For example, the angle between the normal of Phe 18 and that of amide dipoles of residues 41, 77, and 86 increases by 5−8° upon reduction in all proteins. In native and P80A pseudoazurin, the angle with the amide dipoles of residues 76 and 86 also increases by 6−8°. In native and P80A pseudoazurin, the aromatic ring of Phe 18 rotates upon reduction, while the aromatic ring of Phe 33 rotates upon reduction in native and P80I pseudoazurin. In native pseudoazurin, these rotations act to preserve the angle between the normals of the two aromatic rings. However, in P80A and P80I pseudoazurin, these rotations result in a 6° and 10° increase in the angle between the normals to the aromatic planes, respectively. The rotation of these rings together with the shift of the amide dipoles gives the illusion of an expansion of the copper site upon reduction when the oxidized and reduced models are viewed in rapid alternation.

Although Met 7 is not conserved in other cupredoxins [amicyanin (Durley et al., 1993), *Alcaligenes xyloxidans* azurin (Dodd et al., 1995), *Pseudomonas aeruginosa* azurin (Adman & Jensen, 1981), *A. denitrificans* azurin (Baker, 1988), *M. extorquens* pseudoazurin (Inoue et al., 1994), poplar plastocyanin (Guss et al., 1986), *C. reinhardtii*

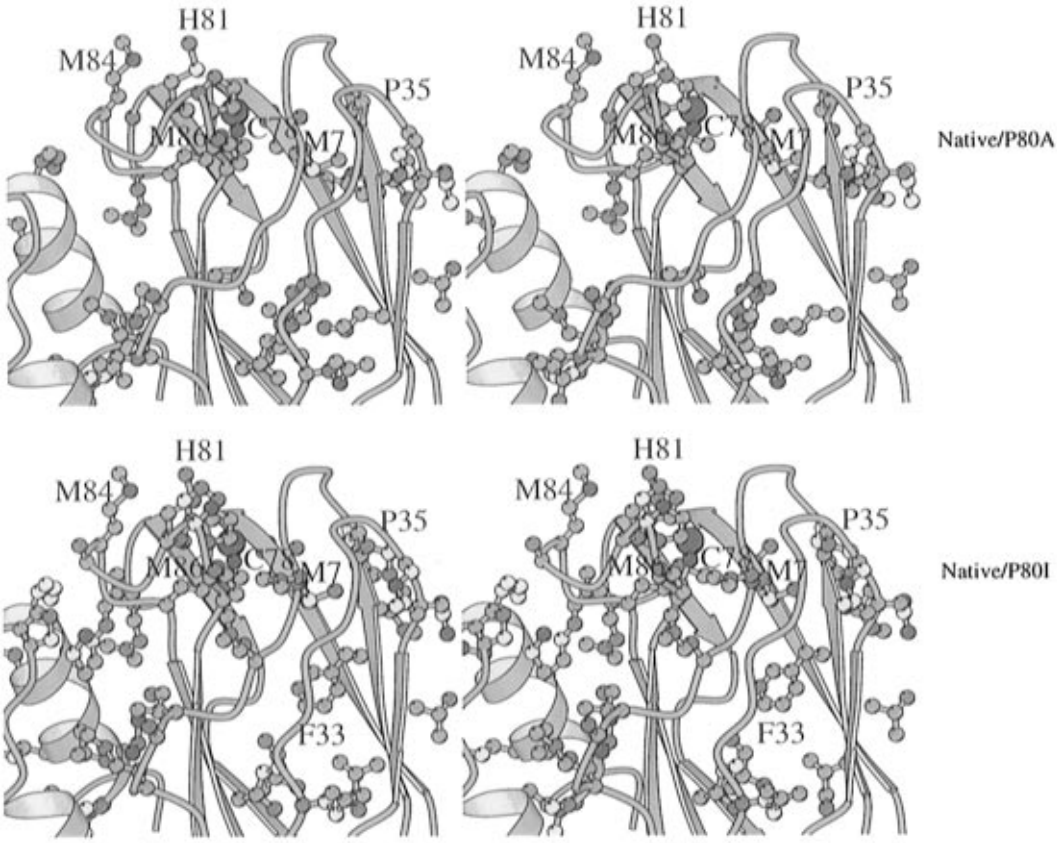

FIGURE 11: Stereoview of the comparison between the oxidized models of native and P80A pseudoazurin (top) and native and P80I pseudoazurin (bottom). The atoms are colored so that blue is a probability of difference less than 25%, green is between 25% and 50%, yellow is 50−70%, and red is greater than 70%. Only residues that contain at least one atom with a probability of difference greater than 30% are shown. For a definition of the probability of difference, see Libeu and Adman (1997). The disordered lysines are not shown. No significant differences are outside the field of the picture.

Table 7: Sulfur−Aromatic and Aromatic−Aromatic Interactions[a]

	units	F18 F33	F18 M7	F18 M86	F33 M7	H40 M16	H81 M16	H81 M84	M16 M84	M16 M86
oxidized native	Å	5.8	**5.1**	**5.2**	**5.8**	4.9	3.7	**4.8**	**5.1**	4.8
	deg	77	**24**	**66**	**60**	61	6.3	**50**	**51**	165
reduced native	Å	5.9	**5.1**	**5.2**	**5.6**	4.9	3.8	**4.9**	**5.2**	4.7
	deg	77	**150**	**70**	**81**	60	8.8	**56**	**64**	169
oxidized P80A	Å	**6.0**	5.0	5.2	5.8	4.9	3.8	**5.0**	5.1	4.9
	deg	**77**	24	63	58	57	2.7	**91**	91	156
reduced P80A	Å	**6.0**	5.1	5.4	5.8	4.8	3.7	**5.0**	5.3	4.8
	deg	**83**	23	60	60	59	1.8	**89**	90	156
oxidized P80I	Å	**6.1**	4.9	5.2	5.9	4.9	3.5	**4.7**	4.9	**4.8**
	deg	**74**	17	69	58	58	3.9	**77**	70	**163**
reduced P80I	Å	**6.1**	4.9	5.3	5.9	4.8	3.7	**4.9**	5.3	**5.0**
	deg	**84**	17	69	58	58	3.3	**69**	75	**148**

[a] Values in boldface mark the interactions that are significantly different between oxidation states. The error in the calculated angles was estimated to be approximately the error in the H40−Cu−H81 bond angle for each model. For the aromatic−aromatic interactions, the distance of the interaction is the distance between the center of mass of the rings, and the angle of interaction is the angle between the normals to the plane of the rings. In the case of the amide dipoles, the distance of interaction is between the center of the nitrogen−carbon bond and the center of mass of the aromatic rings. The angle of interaction is the angle between the normal of the aromatic ring and the normal of the peptide bond minus 90°. The plane of the amide bond was calculated using the amide nitrogen, the C^{α} bonded to the amide nitrogen, the carbonyl carbon, and the carbonyl oxygen. For sulfur−aromatic interactions, the distance of the interaction is the distance between the center of mass of the ring and the sulfur atoms. The angle of interaction is the angle between the normal of the aromatic ring and the normal of the plane determined by the C^{γ}, S^{δ}, and C^{ϵ} of the methionine side chain. For Cys 78, the angle of interaction was calculated using the normal to the plane determined by the Cu and the S^{γ} and C^{β} atoms of the cysteine side chain.

plastocyanin (Redinbo et al., 1993), *Enteromorpha prolifera* plastocyanin (Collyer et al., 1990), and rusticyanin (Walter et al., 1996)], there is always an aromatic residue directly underneath the methionine ligand in a position analogous to Phe 18, consistent with an earlier observation (Adman, 1985) that there is always either an aromatic pair or an aromatic/Met pair of residues that bracket the Met ligand. Even in stellacyanin (Hart et al., 1996) where the methionine ligand is replaced by a glutamine, the glutamine is directly over the ring of a tryptophan. The distance is well conserved and ranges from 4.8 to 5.5 Å, while the angles between normals range from 42° in amicyanin to 98° in *P. aeruginosa* azurin. The aromatic ring is also in the proper geometry to interact with the dipole of the amide of the methionine ligand

Table 8: Selected Interactions between π/σ Orbitals and Amide Dipoles[a]

π/σ orbital			F18			H40[b]			C78			M86[b]
amide dipole	41	76	77	86	87	16	39	40	41	80	81	16
oxidized native	5.7	**5.6**	**5.1**	**4.8**	**4.7**	4.8	**4.3**	**4.3**	5.0	**4.7**[c]	5.7	3.7
	−8.0	**16**	**−2.8**	**4.8**	**23**	−39	**−2.9**	**−40**	−61	**−25**	−72	−77
reduced native	5.8	**5.5**	**5.0**	**4.8**	**4.6**	4.9	**4.4**	**4.4**	5.0	**4.4**[c]	5.4	3.4
	−5.4	**21**	**1.7**	**11**	**28**	−41	**−10**	**−33**	−60	**−17**	−71	−76
oxidized P80A	**5.7**	**5.5**	**5.0**	**4.7**	**4.6**	4.9	4.2	4.4	**5.2**	**4.4**	5.6	**3.8**
	−8.6	**16**	**−1.0**	**7.8**	**25**	−43	−16	−35	**−57**	**−26**	−69	**−80**
reduced P80A	**5.6**	**5.4**	**5.1**	**4.7**	**4.6**	4.8	4.2	4.4	**5.1**	**4.3**	5.6	**3.9**
	−0.4	**24**	**6.8**	**16**	**32**	−41	−17	−33	**−62**	**−18**	−69	**−74**
oxidized P80I	**5.8**	5.6	**5.1**	**4.8**	4.7	4.9	**4.4**	4.3	5.0	4.3	5.6	**3.8**
	−3.6	18	**2.6**	**9.2**	28	−42	**−2.5**	−36	−64	−26	−72	**−76**
reduced P80I	**5.8**	5.5	**5.1**	**4.8**	4.5	4.8	**4.4**	4.3	5.9	4.3	5.5	**4.0**
	1.2	20	**7.8**	**14**	30	−42	**−15**	−38	−67	−25	−69	**−69**

[a] Entries are distances (in Å) between the center of the peptide dipole and the planes defined in Table 7 and angles (in deg) between normals to these planes and the peptide dipole. Values in boldface are where significant changes in the angle occur between oxidation states. [b] H40 and M86 interact only with amide dipole 16. [c] These numbers represent the geometry of the interaction with the amide dipole of residue 80 if residue 80 was not proline, but in the same geometry.

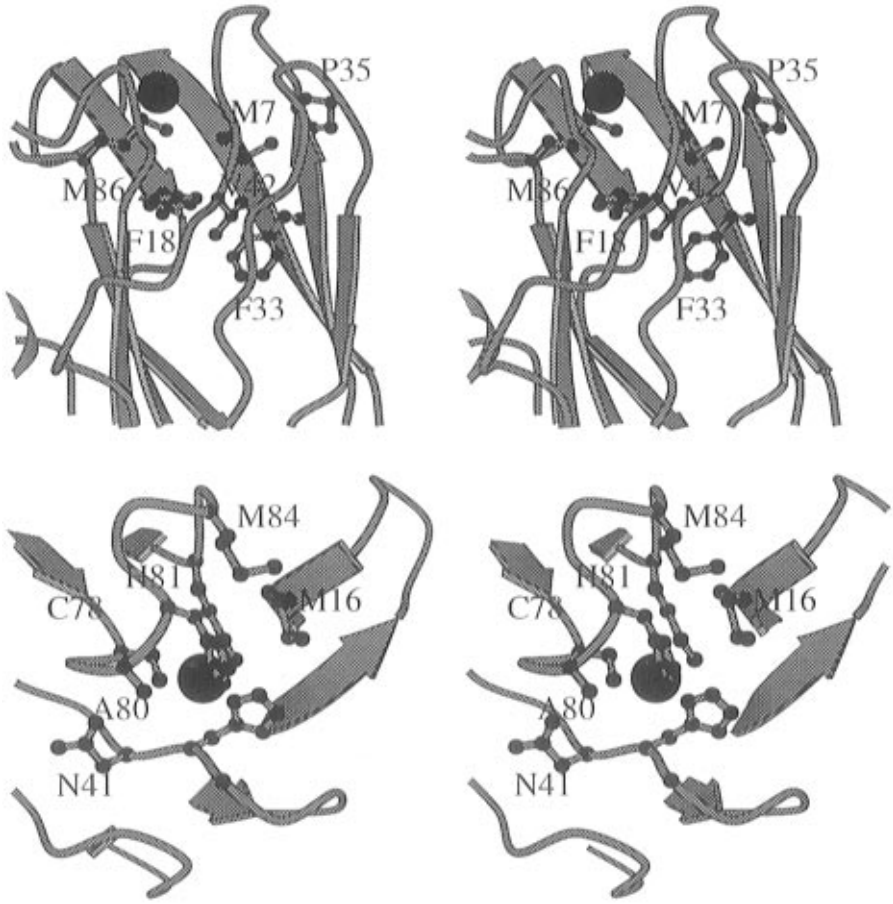

FIGURE 12: Weak electrostatic interactions in pseudoazurin. (Upper) Packing of Phe 18 within the β-barrel. The direction of the 77−78 amide dipole is in the plane of the ribbon just above the label F18 and directed upward toward the copper, that for amide 86−87 is in the plane of the ribbon just below the symbol for M86 and directed away from the copper. (Lower) Weak electrostatic interactions involving the ligand histidines.

in each structure. This interaction appears to be a general feature of cupredoxins.

Both ligand histidines and the cysteine also participate in weak electrostatic interactions; however, these do not change between oxidation states. The interaction between His 81 and Met 16 has the most optimal geometry of any of the weak electrostatic interactions near the copper. The normal of Met 16 is essentially parallel to the normal of His 81. The interaction distance at 3.8 Å is near the mode of observed (Singh & Thornton, 1992) methionine−histidine distances. Near parallel alignment of the normal vectors has been observed in less than 5% of methionine−histidine interactions tabulated in a survey of the Protein Data Bank (Singh & Thornton, 1992). His 40 has a relatively weak interaction with the amide dipole of residue 16 (the angle is neither parallel nor perpendicular). Both interactions are preserved in all six models. This interaction is also found in PMY pseudoazurin, amicyanin, and *A. xyloxidans* azurin. In rusticyanin, the analogous histidine is stacked between two phenylalanine rings.

S^{γ} of Cys 78 is very close to the amide dipole of residue 80. In azurins alone, the cysteine makes a hydrogen bond with this amide nitrogen (Adman, 1991). Although the distance in the mutant pseudoazurins at 4.4 Å is too far for good hydrogen bonding, the alignment of the normal vectors is near optimal for a weak electrostatic interaction. In P80A pseudoazurin, the shift of the cysteine side chain improves the interaction angle between the amide dipole and the cysteine decreasing from −26° to −18° upon reduction. Although the changes in angle are small, the stronger interaction is consistent with a slight increase of charge on the cysteine after reduction of the copper center and the movement of the new water molecule toward the surface of the cleft. For all the blue copper proteins surveyed, the cysteine ligand has a weak electrostatic interaction with other amide dipoles of the triligand loop, inasmuch as they are somewhat aligned in a short helix. The number of interactions is directly related to the length of the loop, and the tighter the turn, the closer the amide dipoles are to the cysteine ligand.

Looking at the entire pattern of weak interactions in Tables 7 and 8, it becomes clear that P80I pseudoazurin has fewer significant changes in the weak interactions than either native or P80A pseudoazurin, consistent with the high redox potential of P80I pseudoazurin, since fewer changes in the weak interactions as well as in the hydrogen bonds imply a lower relaxation energy. The presence of multiple optimally oriented dipole interactions suggests that these may also be functionally relevant to the kinetics of electron transfer.

(C) POLARIS Calculations. For each comparison between the mutant and native pseudoazurins, a complex pattern of structural changes has been observed. In each comparison, there are a few easily detectable structural changes primarily associated with accommodation of the mutation and a myriad of tiny structural changes that seem to form consistent patterns of change in response to reduction of the copper center. Individually, it is very difficult to assess the effect of these changes on the redox potential. The protein dipole−Langevin dipole method can be used to integrate all of these changes into a single energy, the solvation energy.

(1) Mutant versus Wild Type. Table 9 shows the results of the POLARIS calculations for native, P80A, and P80I pseudoazurin models. Although the variation in the calculated solvation energies between the replicate models is uncomfortably high (±1.0 kcal/mol), some interesting insights in the electrostatics of the copper center can be gained by comparing the results of the oxidized and reduced mutant pseudoazurins with the wild-type pseudoazurins.

The solvation energies are not significantly different between the oxidized pseudoazurins unless crystallographic waters are included in the calculation regardless of which charge set is chosen. Explicit inclusion of the new water results in a significantly more positive solvation energy for oxidized P80A pseudoazurin only in the calculations involving charge set I. The difference in solvation energy between oxidized P80A and oxidized native pseudoazurin is 2.5 kcal/mol while the difference between the "replicate" oxidized native pseudoazurins is −0.9 kcal/mol. The increase in solvation energy due to the addition of the new water agrees well with the increase in solvation energy of 3.2 kcal/mol that is equivalent to the observed 139 mV increase in redox potential. However, adding a water does not necessarily increase the solvation energy: when the water bonded to His 81 is included, the energy decreases by −4.9 kcal/mol for the oxidized comparison [Table 9: P80A (b) − native (b)].

Table 9: Solvation Energy for Two Charge Sets[a]

		I		II	
		ΔG	$\sigma(\Delta G)$	ΔG	$\sigma(\Delta G)$
oxidized native	a	−25.23	0.02	−35.13	0.05
	b	−23.74	0.02	−35.78	0.05
oxidized native (1paz)	a	−26.13	0.02	−33.83	0.09
reduced native	a	−21.58	0.02	−33.45	0.10
	b	−23.24	0.01	−33.81	0.10
reduced native (1pza)	a	−24.3	0.01	−33.83	0.09
oxidized P80A	a	−26.26	0.02	−36.31	0.08
	b	−28.67	0.02	−34.42	0.08
	c	−22.73	0.02	−34.12	0.08
reduced P80A	a	−26.56	0.02	−35.62	0.09
	b	−26.00	0.02	nc	nc
	c	−25.77	0.03	−34.42	0.08
	d	−21.00	0.02	nc	nc
oxidized P80I	a	−25.13	0.02	−34.94	0.12
	b	−25.11	0.02	nc	nc
reduced P80I	a	−23.92	0.01	−34.83	0.09

[a] The different calculations are protein only (a), protein plus the water bound to His 81 (b), protein plus the new water (c), and protein plus the new water with hydrogens oriented differently (d). $\sigma(\Delta G)$ is the variation in the solvation energy for 15 different grid choices. The charges for charge sets I and II are shown in Table A-1 of the Supporting Information. nc = not computed. The energies are in kcal/mol.

These effects are smaller for charge set II, in part due to the lower net charge of the copper center. The effect of a lower charge can be seen by decreasing the charge on each ligand by 0.25 e and monitoring the potential energy between the charges in the copper center and the fixed dipoles of the protein [see Figure 6 in Libeu (1996)]. Basically, residues that are closest to the changed charges are affected the most. In addition to directly affecting the charge−fixed dipole contributions to the overall solvation energy, different charge sets also affect the orientation of movable hydrogens. Without water, all three pseudoazurins have the same movable hydrogens so that effects due to their placement roughly cancel out when calculations between pseudoazurins are compared. When a water molecule is explicitly added to one of the models, then the difference in solvation energy has a component which is the difference in the electrostatic interaction between the water molecule with the partial charges of the closest ligands and the copper which, if all other things are equal, dominates the difference in the solvation energy between the native and mutant protein. The effect of adding the water bound to His 81 is almost always smaller than the effect of adding the new water simply because the water bound to His 81 is 6.7 Å away from the copper atom compared to 4.7 Å for the new water, but more importantly, the new water is *unique* to the P80A form.

Inclusion of a correctly oriented new water is sufficent to explain most of the increase in redox potential of the P80A mutant (139 mV = 3.2 kcal/mol). The most reasonable hydrogen bonding of the new water molecule is produced for both oxidized and reduced forms of P80A by using charge set I, which has a more negatively charged Cys that creates an electric field at the position of the new water with sufficient gradient to orient the hydrogens. In the oxidized orientation, the lone pair of the new water makes a weak N−H···O bond with the amide of Ala 80, and one of the hydrogens points toward the $O^{\delta 1}$ of Asn 41 for a good O−H···O bond. The final hydrogen points almost directly

at the S^{γ} of Cys 78. In the reduced orientation the hydrogen on the new water is only in a reasonable position to make a hydrogen bond with the carbonyl oxygen of Gly 39. Using charge set II, one of the hydrogens is directed at the copper center, but neither hydrogen is in the proper geometry to make a good hydrogen bond with Asn 41. Yet a third orientation is found for hydrogens on the new water if all the other crystallographic waters are included using charge set I. Repeating the POLARIS calculations using the new orientation of the new water [Table 9, P80A (d)], the solvation energy decreases 5 kcal/mol. The solvation energy is very sensitive to the orientation of the water in both the oxidized and reduced forms. Unfortunately, the orientation of the hydrogens is not available from the crystallographic experiment.

(2) Comparison of the Oxidized and Reduced Pairs. In the absence of solvent, the solvation energy of the reduced native pseudoazurins is more positive than or equal to the solvation energy of their companion oxidized pseudoazurin and is nearly independent of the charge set chosen (Table 9). The presence of crystallographic waters complicates the comparison because of the different number of waters used in each comparison. In P80A pseudoazurin, inclusion of the new water molecule tends to amplify the differences in solvation energy. Although small, the increase in solvation energy upon reduction is consistent with the positive redox potential of the pseudoazurins.

In native and P80A pseudoazurin, the increased solvation energy of the reduced pseudoazurins most likely results from the movement of the copper atom upon reduction. The difference in the solvation energy between the oxidized and reduced models is almost entirely due to a difference in the charge−fixed dipole term. Interactions between ligands and protein atoms contribute to charge−induced dipole and charge−solvent contribution by orienting the Langevin dipoles. The POLARIS calculations allow one to examine contributions from individual residues to different terms. In native pseudoazurin, large differences in contributions to the charge−fixed dipole term are seen [Figure 8 in Libeu (1996)] for Met 7, Met 16, Ile 34, Lys 38, Asn 63, Thr 79, and Ser 104. Of these, Lys 38, Asn 63, and Ser 104 are modeled as two conformations with different highest occupied configuration in oxidized and reduced pseudoazurin models. However, compensating differences in the induced electric field particularly due to differing orientations of the Langevin dipoles (Stephens et al.,1996) drastically reduce the effects of these surface residues. In contrast, the amide dipoles of Met 7, Met 16, and Thr 79 are relatively close to the copper center and buried within the protein. Here differences in the charge−dipole interactions are seen because these amide dipoles and the copper atom have moved relative to each other, as for example for Met 7 S^{δ}. (This additional energy is not the $\sigma-\pi$ weak electrostatic interaction discussed earlier but a contribution to the Coulomb energy from the partial charge on the sulfur atom.) The amide dipole of Ala 80/Ile 80 is also close enough to interact with the copper as shown by the relatively large reorientation observed in both P80A and P80I pseudoazurin. Met 16, Gly 39, Asn 41, and either Thr 79 or residue 80 interact strongly with the copper in all three pseudoazurins. The consistency of these results indicates that these residues are important in determining the electric field at the copper center and are important contributors to the solvation energy. The modest increase in redox potential between both M16F (+43 mV) and T79V (+55 mV) (unpublished data) and native pseudoazurin may thus be partly due to reorientation of the amide dipoles of these residues with respect to the copper atom.

The difference in solvation energy represents the relative ability of the fixed models to stabilize the reduced copper center. Qualitatively, the solvation energy appears to be inversely correlated with the increasing trigonality of the copper center. This added stability should not be confused with the increased stability of the trigonal form due to quantum mechanical effects predicted by Solomon (1983). In the present calculation extra energy appears to come from the concerted movement of the cysteine sulfur and the copper toward a more buried position upon reduction, which has more favorable interactions with the surrounding amide dipoles.

DISCUSSION

In this work the goal was to understand how a specific sequence difference in pseudoazurin acts to tune the redox potential of the copper, in particular, how the P80A and P80I mutations increase the redox potential of pseudoazurin by +139 and +180 mV, respectively. In order to accomplish this goal, native, P80A, and P80I pseudoazurin structures have been determined in two oxidation states, and the solvation energy of the copper center has been calculated for all six forms. Although the two mutations are very similar, the mechanism through which the redox potential is increased appears to be different between the two mutants.

The structural studies indicate that overall all three pseudoazurins are extremely similar in both oxidation states. The weighted root mean square deviations between all the final models are between 0.11 and 0.16 Å. However, in addition to a general increase in displacement parameters upon reduction, (reversible) distinct patterns of change are seen at the copper site in all three pseudoazurins. There are only four consistent structural responses to reduction: the copper moves to a more trigonal position (Cu−S^{δ} lengthens), Met 7 and Pro 35 move coordinately, and the weak electrostatic interactions between His 81 and Met 16 and the weak electrostatic interactions between Phe 18 and the amide dipoles of residue 77 and 86 change. Except for the concerted change in Met 7 and Pro 35, all of these changes are also observed in plastocyanin, indicating that these differences may represent a general response for the plastocyanin-like cupredoxins.

A difference in structure analogous to the change at Met 7 and Pro 35 is not observed in plastocyanin because the residue equivalent to Met 7 is an isoleucine and thus lacks the weak interaction between Met 7 and Phe 18. In all cupredoxins with models in the Protein Data Bank, an aromatic residue is found in the position in the barrel occupied by Phe 18 located directly underneath the methionine ligand of the copper. The strength of the $\sigma-\pi$ interaction ranges from optimal in amicyanin to none in *P. aeruginosa* azurin. In pseudoazurin, the sulfur of Met 7 is positioned for a near optimal $\sigma-\pi$ interaction, while the sulfur of Met 86 is positioned about half way between the extrema of the $\sigma-\pi$ interaction. Since these interactions are very sensitive to the ambient electric field (Cheney et al., 1989), the change of the electric field at the copper center may be transmitted through Met 86 to increase the coupling between Met 7 and Phe 18.

Beyond these four changes, there is a host of complex changes involving (1) hydrogen bonds among the main chain

atoms of the ligand residues and betweenThr 79 and Asn 41, (2) weak electrostatic interactions, and (3) two specific water molecules. In general, the pattern of changes is more similar between mutants than between either mutant and native. This similarity appears to be the result of the altered geometry of the copper center in the mutant pseudoazurins. In the reduced states of P80A and P80I pseudoazurin, the copper is significantly closer to the plane determined by the cysteine and histidine ligands than in either oxidation state of native pseudoazurin. Since the ϕ, ψ angles of prolines are more restricted than either those of alanine or isoleucine, mutation of the proline presumably allows the protein to relax into a conformation that is not accessible to the native protein in response to reduction.

The mutant pseudoazurins are the first cupredoxins (with unmutated ligands) in which a significant change in the geometry of the copper center has been observed upon reduction at constant pH. That the geometry is more favorable to Cu^{1+} than Cu^{2+} agrees with the rack-induced bonding hypothesis introduced by Fee and Malmström (1968). They suggested that the positive redox potentials of the cupredoxins, the characteristic blue color, and the unusual hyperfine splitting are due to the tertiary structure of the protein forming a chelating site with very little flexibility. A copper atom bound in this site would be forced to adopt a conformation poised between the favorable geometries for Cu^{2+} and Cu^{1+}. The geometry of the copper changes relatively little upon reduction in the native cupredoxins whose structures have been determined in both oxidation states at approximately pH 7.0: poplar plastocyanin (Guss et al., 1986), pseudoazurin (Vakoufari et al., 1994; this study), and *Alcaligenes faecalis* azurin (Shepard et al., 1990). In contrast, in both P80A and P80I pseudoazurin the copper geometry is significantly more trigonal in the reduced state than in the oxidized.

The increased accommodation of the Cu^{1+} preferred geometry contributes to the higher redox potential of the mutant pseudoazurins over the native and is the result of changing only a single residue. The mutations which confirm the rack hypothesis apparently slightly destabilize the rack. This increased trigonality should stabilize the reduced copper better than the reduced states found in native pseudoazurin or native plastocyanin, but not *A. denitrificans* azurin. Both oxidation states of *A. denitrificans* azurin are even more trigonal than the reduced P80A or P80I pseudoazurin even though all three lack the proline conserved in plastocyanin-like cupredoxins. The trigonality of the copper site is thus not due to this sequence difference alone. In all azurins whose structures have been determined to date, there is a carbonyl oxygen within the coordination sphere of the copper in the oxidized forms, an extra NH−S hydrogen bond between the analogous amide of residue 80 and the cysteine S^{γ}, and a longer triligand loop in the azurins than the plastocyanin-like cupredoxins (Adman, 1991). These structural differences may be an indication that the unique geometry of the copper center is stabilized by slightly different forces in the azurins than in the plastocyanin-like cupredoxins.

Geometrical stabilization of Cu^{1+} is not the only mechanism outside the copper site which may contribute to the increased redox potentials. The water that fills the dimple in the protein surface created by the P80A mutation provides an extra movable dipole that is not present in either native or P80I pseudoazurin. Electrostatic calculations indicate that the presence of this extra dipole decreases the solvation energy of the copper center in the P80A pseudoazurin enough to explain the observed increase in redox potential. The water molecule bound to $N^{\epsilon 1}$ of His 81 is another example of a movable dipole which may affect the solvation energy of the copper center. The water molecule has distinctly different behavior in response to reduction in all three pseudoazurins: it is unaffected by reduction in native pseudoazurin, makes a weaker hydrogen bond with His 81 in reduced P80A pseudoazurin than oxidized P80A pseudoazurin, and disappears in reduced P80I pseudoazurin. Together with the amide dipoles of the triligand loop, these water molecules are the closest dipoles to the copper center, which implies that not only do they have the greatest effect on the solvation energy of the copper center but they also greatly contribute to the electric field of the copper center. It is perturbations in this electric field which determine the relative energies for the different geometries of the copper center and hence how much geometrical stabilization of Cu^{1+} can occur in each protein. In this manner, differences in the solvation of the copper center in all pseudoazurin contribute to the differences in their redox potential if only indirectly.

Particularly for the mutant proteins, the lower resolution of the models makes detecting changes between the oxidation states and between the native and mutant models difficult. One very important consequence of the P80I mutation is that the quality of the P80I crystals is lower than for either P80A crystals or native pseudoazurin crystals. The limit of diffraction is 2.0 Å for oxidized P80I crystals and 2.2 Å for reduced P80I crystals. The lower resolution of the P80I models creates the impression that there are fewer differences between the oxidation states for P80I pseudoazurin than for P80A or native pseudoazurin, when many of these differences may be obscured by the relatively poorer resolution of the models.

The best interpretation of the crystallographic experiments combined with the calculation of the solvation energies is that altered solvation of the copper center does not account for the very high redox potential of P80I pseudoazurin. P80I pseudoazurin has the most trigonal copper center geometry in both forms, so that geometrical stabilization of the reduced copper may be the most important effect. For P80A pseudoazurin, the altered solvation may play a significant role in the increased redox potential, in addition to a contribution from geometrical stabilization of the copper site.

The P80A and P80I mutants have demonstrated two distinct effects. Sequence difference may allow the protein to be more flexible and thereby accommodate the reduced copper in a binding site significantly more trigonal than the oxidized binding site. In addition, the POLARIS results indicate that addition of a single dipole 4.5 Å from the copper can change the solvation energy of the copper center by a sufficient magnitude to account for a redox potential change of 100−200 mV.

ACKNOWLEDGMENT

Data collection by Stewart Turley, help with the POLARIS calculations from Bill Parson, and discussions with Dave Teller, Bill Parson, and Ethan Merritt are gratefully acknowledged.

SUPPORTING INFORMATION AVAILABLE

A brief description of the rationale for the parameters used in the POLARIS calculations, the actual charges for the copper center, and a description of the effects of changing charges on the ligands (9 pages). Ordering information is given on any current masthead page.

REFERENCES

Adman, E. T. (1985) in *Topics in Molecular and Structural Biology. Vol. I, Metalloproteins* (Harrison, P., Ed.) pp 1−42, Macmillan, New York.

Adman, E. T. (1991) *Adv. Protein Chem. 42*, 145−97.

Adman, E. T., & Jensen, L. H. (1981) *Isr. J. Chem. 21*, 8−12.

Adman, E. T., Turley, S., Bramson, R., Petratos, K., Banner, D., Tsernoglou, D., Beppu, T., & Watanabe, H. (1989) *J. Biol. Chem. 264*, 87−89.

Baker, E. N. (1988) *J. Mol. Biol. 203*, 1071−1095.

Bernstein, F. C., Koetzle, T. F., Williams, G. J. B., Meyer, E. F., Bruce, M. D., Rodgers, J. R., Kennard, O., Shimanouchi, T., & Tasmui, M. (1977) *J. Mol. Biol. 112*, 535−542.

Blackwell, K. A., Anderson, B. F., & Baker, E. N. (1994) *Acta Crystallogr. D50*, 263−270.

Bouwman, E., Dreissen, W. L., & Reddijk, J. (1990) *Coord. Chem. Rev. 104*, 143−172.

Brünger, A. T. (1990) *X-PLOR Version 3.1*, Yale University, New Haven, CT.

CCP4, Collaborative Computational Project Number 4 (1994) *Acta Crystallogr. D50*, 760−763.

Cheney, B. V., Schulz, M. W., & Cheney, J. (1989) *Biochim. Biophys. Acta 996*, 116−124.

Church, W. B., Guss, J. M., Potter, J. J., & Freeman, H. C. (1986) *J. Biol. Chem. 261*, 243−257.

Churg, A. K., & Warshel, A. (1986) *Biochemistry 25*, 1675−1681.

Collyer, C. A., Guss, J. M., Sugimura, Y., Yoshikazu, F., & Freeman, H. C. (1990) *J. Mol. Biol. 211*, 617−632.

Connolly, M. L. (1983) *Science 221*, 709−713.

Dodd, F. E., Hasnain, S. S., Hunter, W. N., Abraham, Z. H., Debenham, M., Kanzler, H., Eldridge, M., Eady, R. R., Ambler, R. P., & Smith, B. E. (1995) *Biochemistry 34*, 10180−10186.

Durley, R., Chen, L., Louis, L. W., Mathews, F. S., & Davidson, V. I. (1993) *Protein Sci. 2*, 739−752.

Engh, R. A., & Huber, R. (1991) *Acta Crystallogr. A47*, 392−400.

Fee, J. A., & Malmström, B. G. (1968) *Biochim. Biophys. Acta 153*, 299−302.

Garrett, T. P. J., Clingeleffer, D. J., Guss, J. M., Rogers, S. J., & Freeman, H. C. (1984) *J. Biol. Chem. 259*, 2822−2825.

Gluckert, J. A., Lowery, M. D., & Solomon, E. I. (1995) *J. Am. Chem. Soc. 117*, 2817−2844.

Gray, H. B., & Solomon, E. I. (1981) in *Copper Proteins* (Spiro, T. C., Ed.) pp 1−37, Wiley Interscience, New York.

Guss, J. M., Harrowell, P. R., Murata, M., Norris, V. A., & Freeman, H. C. (1986) *J. Mol. Biol. 192*, 361−387.

Han, J., Adman, E. T., Beppu, T., Freeman, H. C., Huq, L. L., Loehr, T. M., & Sanders-Leohr, J. (1991) *Biochemistry 30*, 10904−10913.

Hart, P. J., Nersissian, A. M., Herrmann, R. G., Nalbandyan, R. M., Valentine, J. S., & Eisenberg, D. (1996) *Protein Sci. 5*, 2175−2183.

Hendrickson, W. (1985) *Methods Enzymol. 45*, 149−195.

Higashi, T. (1990) *J. Appl. Crystallogr. 23*, 253−257.

Howard, A. J., Gilliland, G. L., Finzel, B. C., Poulos, T. L., Ohlendorf, D. H., & Salamme, F. R. (1987) *J. Appl. Crystallogr. 20*, 383−387.

Inoue, T., Kai, Y. , Shigeharu, H., Kasai, N., Oshiro, Y., Suzuki, S., Kohzuma, T., & Tobari, J. (1994) *Acta Crystallogr. D50*, 317−328.

Jones, T. A., Zuu, J.-Y., Cowan, S. W., & Kjeldgarrd, M. (1991) *Acta Crystallogr. A47*, 110−119.

Kakutani, T., Watanabe, H., Arima, K., & Beppu, T. (1981) *J. Biochem. 89*, 463−472.

Kukimoto, M., Nishiyama, M., Ohnuki, T., Turley, S., Adman, E. T., Horinuchi, S., & Beppu, T. (1995) *Protein Eng. 8*, 153−158.

Langen, R., Brayer, G. D., Berghuis, A. M., McLendon, G., Sherman, F., & Warshel, A. (1992) *J. Mol. Biol. 224*, 589−600.

Laskowski, R. A., Moss, D. S., & Thornton, J. M. (1993) *J. Mol. Biol. 231*, 1049−1067.

Lee, F. S., Chu, Z. T., & Warshel, A. (1993) *J. Comput. Chem. 14*, 161−185.

Libeu, C. A. P. (1996) Ph.D. Thesis, Chapter 3, University of Washington, Seattle, WA.

Libeu, C. A. P., & Adman, E. T. (1997) *Acta Crystallogr. D53*, 56−76.

Nishiyama, M., Suzuki, J., Ohnuki, T., Chang, H. C, Horinouchi, S., Turley, S., Adman, E. T., & Beppu, T. (1992) *Protein Eng. 5*, 177−184.

Petratos, K., Dauter, Z., & Wilson, K. S. (1988) *Acta Crystallogr. B44*, 628−636.

Petratos, K. Z., Papadovasilaki, M., & Dauter, Z. (1995) *FEBS Lett. 368*, 442.

Redinbo, M. R., Cascio, D., Choukair, M. K., Rice, D., Merchant, S., & Yeates, T. O. (1993) *Biochemistry 32*, 10560−10567.

Russell, S. T., & Warshel, A. (1985) *J. Mol. Biol. 185*, 389−404.

Shapleigh, J. P., & Payne, W. J. (1985) *FEMS Microbiol. Lett. 26*, 275−279.

Sheldrick, G. M. (1993) *SHELXL-93. A Program for Structure Refinement*, University of Göttingen, Göttingen, Germany.

Shepard, W. E. B., Anderson, B. F., Lewandowski, D. A., Norris, G. A., & Baker, E. N. (1990) *J. Am. Chem. Soc. 112*, 7817−7819.

Shepard, W. E. B., Kinston, R. L., Anderson, B. F., & Baker, E. N. (1993) *Acta Crystallogr. D49*, 331−343.

Singh, J., & Thorton, J. M. (1992) *Atlas of Protein Side-Chain Interactions*, Vol. 1, pp 572−573, 524−525, Oxford University Press, Oxford, England.

Solomon, E. I. (1983) in *Copper Coordination Chemistry, Biochemical & Inorganic Perspectives* (Karlin, K., & Zubieta, J., Eds.) pp 1−22, Adenine Press, Guilderland, NY.

Stephens, P. J., Jollie, D. R., & Warshel, A. (1996) *Chem. Rev. 96*, 2491−2513.

Sykes, A. G. (1990) *Struct. Bonding 75*, 176−225.

Vakoufari, E., Wilson, K. S., & Petratos, K. (1994) *FEBS Lett. 347*, 203−206.

Walter, R. L., Ealick, S. E., Friedman, A. M., Blake, R. C., Proctor, P., & Shoham, M. (1996) *J. Mol. Biol. 263*, 730−751.

Warshel, A. (1991) *Annu. Rev. Biophys. Chem. 20*, 267−298.

Wehrfritz, J. M., Reilly, A., Spiro, S., & Richardson, D. J. (1993) *FEBS Lett. 335*, 246−250.

Werst, M. M., Davoust, C. E., & Hoffman, B. M. (1990) *J. Am. Chem. Soc. 113*, 1533−1538.

Wilson, A. J. C. (1976) *Acta Crystallogr. A32*, 994−996.

BI9704111